Stony Brook University

Climatology and Synoptic Evolution of Major Forest Fire Events Over the Northeast U.S.

A Thesis Presented

by

Joseph Benjamin Pollina Jr.

to

The Graduate School

in Partial Fulfillment of the

Requirements

for the Degree of

Master of Science

in

Marine and Atmospheric Science

Stony Brook University

August 2011

Stony Brook University

The Graduate School

Joseph Benjamin Pollina Jr.

We, the thesis committee for the above candidate for the

Master of Science degree, hereby recommend

acceptance of this thesis.

Dr. Brian A. Colle – Thesis Advisor
Professor, School of Marine and Atmospheric Sciences

Dr. Minghua Zhang – Second Reader
Professor, Interim Dean, Interim Director of Marine Sciences Research Center, School of Marine and Atmospheric Sciences, Interim Dean

Dr. Sultan Hameed – Third Reader
Professor, Associate Dean, Director of Institute of Terrestrial and Planetary Atmosphere, School of Marine and Atmospheric Sciences

This thesis is accepted by the Graduate School

Lawrence Martin
Dean of the Graduate School

Abstract of the Thesis

Climatology and Synoptic Evolution of Major Forest Fire Events Over the Northeast U.S.

by

Joseph Benjamin Pollina Jr.

Master of Science

in

Marine and Atmospheric Science

Stony Brook University

2011

This study presents a spatial and temporal climatology of major wildfires (>100 acres burned) in the Northeast U.S from 1999 to 2009 and the meteorological conditions associated with these events. About 59% of the wildfire events in this region occur in April and May, with ~76% of all wildfires over the higher elevation (> 1000 m) regions of the Northeast occurring in these months, while ~53% occur in the Appalachian lee and the coastal plain. The other 41% of wildfires occur in the summer, fall and early spring months.

The synoptic flow patterns associated with Northeast wildfires were classified using the North American Regional Reanalysis (NARR). The most common synoptic pattern in the Appalachian high terrain region is a surface high pressure centered over the northern Appalachians (~46% of events). For the coastal plain fire events, the most common pattern (~46%) is an anticyclone extending southward from southeastern Canada and Great Lakes to the Northeast. Trajectories show that the pre-high pattern shows the greatest subsidence, greatest decrease in relative humidity, and greatest increase in temperature. Terrain sensitivity studies show that there is a 1°C to 2°C increase in temperature and a 0%-8% decrease in RH when there is a southwesterly flow downsloping event over the NEUS.

Dedication Page

This thesis is dedicated to my family and friends, especially my mother and father whose love and support provided the strength I needed to finish this project. This thesis is also dedicated to my partner Mike, who also provided love and support, and stuck with me even through the late nights and darkest hours. These past 5 years have been the toughest of my life, and I'm glad I had him by my side.

Table of Contents

List of Tables

List of Figures

Acknowledgments

I would like to thank the School of Marine and Atmospheric Sciences at Stony Brook University, especially Dr. Brian Colle, whose guidance and expertise was invaluable. I would also like to thank Dr. Jay Charney of the USDA Forest Service in East Lansing Michigan for his input into this study. Finally, I would like to thank the National Weather Service and the New York City Weather Forecast Office for supporting this study and allowing me the time to finish. I would especially like to thank Information Technology Officer, Matthew Sardi, who took many hours out of his busy schedule to help me with the technological portion of this project.

Chapter 1 – Introduction

a. Background

Over 77,000 wildfires per year across the United States burn ~4.7 million acres annually on average (Shein 2009). The relatively arid western U.S. is more prone to large wildfires than the eastern U.S. For example, in 2008 approximately 4.7 million acres burned from wildfires west of the Mississippi River [National Interagency Fire Center (NIFC) 2008], while ~500,000 acres burned east of the Mississippi. Southern California is particularly vulnerable, due to episodic periods of a large-scale ridge over the western U.S. and associated offshore-directed Santa Ana winds (Raphael 2003; Glickman, 2000). In 2008, wildfires in the Northeastern states [Connecticut (CT), Massachusetts (MA), New Hampshire (NH), New York (NY), New Jersey (NJ), Maine (ME), Rhode Island (RI), Vermont (VT), and Pennsylvania (PA)] resulted in 11,792 acres burned, which is ~0.22% of the total acres burned within the contiguous U.S. (NIFC 2008). About 71% of all major wildfires in the Northeast U.S. are caused by humans as opposed to only 1.9% for dry lightning (a major cause of wildfire for the Western U.S. [Rorig and Ferguson 2002]).

Although large wildfires are relatively rare over the eastern U.S, they still can have substantial impacts. For example, the “Sunrise Fire” in late August 1995 burned ~7,000 acres across portions of the Pine Barrens region of eastern Long Island (Hamilton and Ostapow 2009), destroying a house, 5 fire trucks, and damaging nine other houses and several businesses. The cost of the fire was $2-3 million (Hamilton and Ostapow 2009). Soon after this fire the New

York Wildfire and Incident Management Academy was created in Suffolk County, NY to train forest rangers and local fire departments in effective fire and land management (Tim Morrin, National Weather Service, personal communication 2009).

On 17 April 2008, the "Overlooks" wildfire burned over 3,000 acres in Minnewaska State Park Preserve near New Paltz, NY. The spread of the fire was aided by relatively dry conditions (20-25% relative humidity). Forest rangers were forced to close all roads in the 20,000 acre park, and the wildfire was not contained until 22 April 2008 (Buckley 2008). It was the largest fire in the park during the last 60 years.

b. *Fire weather forecasting*

In addition to the topography and available surface fuels for wildfire ignition and behavior, a forecaster has to consider several meteorological ingredients for wildfire threat, such as near surface temperature, relative humidity (RH), wind speed and direction, precipitation, and atmospheric stability. Higher air temperature increases the probability that fuels will reach their ignition temperature (Parr et al. 2005, Kassomenos 2010). In addition, the moisture content of the fuels tends to decrease as the surface temperature increases and the RH decreases, thus increasing the potential for a wildfire. Low-level winds control the rate and direction of fire spread (Parr et al. 2005).

An important component of the National Weather Service's (NWS) effort to protect life and property is the anticipation of wildfire threat days. A distinction between actual wildfires and wildfire threat needs to be made to avoid confusion. Actual wildfires are days in which wildfires were observed, while wildfire threat describes the *potential* for the ignition and spread of wildfires.

There are two common methods used to assess and communicate wildfire threat to the general public. The first method used to forecast wildfire threat is the National Fire Danger Rating System (NFDRS) (Werth 2003). NFDRS is a model that uses topographical data, meteorological data from Remote Automated Weather Stations (RAWS), as well as fuel data as inputs, and outputs a rating to describe wildfire threat, such as low, moderate, high, very high, and extreme. This adjective rating helps the fire community prepare for the potential of a wildfire. For example, an increase from a moderate to a high adjective rating means that the fire community should increase their staff (Werth 2003).

The second method of assessing and communicating a wildfire threat is through the issuance of Fire Weather Watches (FWW) or Red Flag Warnings (RFW). The NWS issues FWWs or RFWs for an area when certain pre-defined meteorological criteria favoring wildfires are met. For example, at the New York City Weather Forecast Office (WFO), an FWW or RFW is issued in the spring, fall, and winter when the sustained surface winds or gusts exceed 11.2 m s^{-1} (21.7 kts), RH is < 30%, and the rainfall is < 0.25" during the last three days. During the summer, the criteria is the same except rainfall must be < 0.25" during the last 5 days, and the Keetch-Byram Drought Index (Keetch and Byram 1968) must be above 300 (National Weather Service, New York City, 2008). These are the criteria used by the New York City National WFO, but the FWW and RFW criteria can vary regionally (Tim Morrin, personal

communication 2010). The differences between an FWW and an RFW are time of issuance and forecaster certainty of the conditions. An FWW is issued 24 to 72 hours prior to an event with forecaster certainty of greater than 30% but less than 70%. An RFW is issued within 24 hours of an event and forecaster certainty of greater 70%. The criteria to issue FWWs or RFWs come from numerical weather prediction (NWP). Since the 2 different threat approaches are achieved differently, the end result may be different. For example, FWWs and RFWs may only occur a few times a year, while a NFDRS rating of "high" or greater may occur several times in one year.

A few studies have explored the ingredients that increase wildfire threat over the Northeast U.S. In many cases, wildfires occur under high pressure and associated subsidence drying (Schaefer 1957). For some events the descent of strong winds and drying from the middle-troposphere to the boundary layer can enhance the potential for a fire to spread (Schaefer 1957, Charney and Keyser 2009). For example, the Double Trouble State Park fire in central New Jersey on 2 June 2002 occurred in the late afternoon immediately following the passage of a dry and gusty cold front (Charney et al. 2003). Kaplan et al. (2008) and Charney and Keyser (2009) noted an intrusion of dry air from ~550 hPa to ~750 hPa, which was mixed to the surface within the deep convective boundary layer and thus created another period of drying behind the front. The mid-level dry air during this Double Trouble event descended within the equatorward (right) exit region of a jet streak (Kaplan et al. 2008).

c. *Fire weather synoptic patterns*

Several studies have related the synoptic atmospheric patterns to actual wildfires or wildfire threat. In a report for the U.S. Forest Service, Schroeder et al. (1964) categorized the synoptic flows for critical fire weather ingredients across the lower 48 U.S. states from 1951 to 1960. They showed that for the Northeast U.S., high fire threat is associated with 4 types of pressure systems: Canadian high, Pacific high, Bermuda high, and Atlantic storm. If the high passes to the north of the Northeast region, high fire danger usually occurs after the passage of a cold front. If the high pressure center passes to the south, high fire danger usually occurs before the passage of a cold front on the western or northern side of the high. If there is a westward extension of the Bermuda high into the southern U.S., the advection of low-level moisture from the Gulf of Mexico can be limited.

Takle et al. (1994) used a synoptic weather classification system developed by Yarnal (1993) to highlight the different types of surface high and low pressure patterns associated with actual wildfire events in West Virginia (WV). Of the eight different Yarnal types of surface pressure patterns, Takle et al. (1994) found that the western side of a departing high pressure system was the most common pattern for wildfires in WV. Also, a surface high pressure centered to the south contributes to drying conditions in WV due to westerly downslope flow in the lee of the Appalachians.

Newark (1975) associated a persistent (~55 days) long-wave ridge at mid-levels with one of the worst wildfire seasons on record in Canada in the northwest portions of the province of Ontario in the summer of 1974. Skinner et al. (2002) presented a several decade climatology of

wildfires for all Canadian provinces with the exception of the 4 eastern Atlantic provinces and found that the fires are associated with a northward and eastward extension of anomalously high geopotential heights at 500 hPa and a deeper than normal west coast 500 hPa trough. Finally, Kassomenos (2010) found that wildfires over Greece are favored when a surface low pressure system intensifies and increases the pressure gradient (winds), or when there is a gradual transition from low to high pressure. The high temperatures, low humidity, and moderate wind speeds associated with a building high contributes to the onset and longevity of these wildfires.

d. *Motivation*

While there have been some case studies investigating fire weather events over the Northeast U.S. (hereafter referred to as NEUS and includes the following states: PA, NJ, NY CT, RI, MA, VT, NH, and ME) (e.g. Charney and Keyser 2008; Charney et al. 2003; and Kaplan et al. 2008), no extensive climatologies over the NEUS have been published. Schroeder et al. (1964) presented an analysis of the synoptic types for Northeast wildfires, but they only concentrated on "critical fire weather" (they sectorized the U.S. and subjectively assigned fire load threshold values for the different sections of the U.S. to define critical fire weather) in an unpublished report, and not actual wildfires. Also, they do not consider as many synoptic patterns as may exist for these events. They also do not divide the NEUS into smaller regions in order to better understand the impact of the local terrain.

Figure 1.1 shows the population density and degree of forestation for the NEUS (U.S. Forest Service 2010). Outside of the heavily populated, nonforested metro areas of the NEUS such as New York City, Northeast New Jersey, eastern MA, and southeast PA, the coastal plain of the NEUS is a heavily populated forested region, which can be sensitive to the effects of wildfires. Small wildfires (compared to the Western U.S.) can have a large impact. Given the impact that wildfires can have on life and property, especially across the highly populated region of the NEUS, it is important to better understand the ambient conditions that increase the likelihood of wildfires in this area. A comprehensive fire weather climatology will help forecasters recognize the features that are associated with the increased risk of NEUS wildfires. In particular, this research will address the following questions:

- Where are wildfires favored across the NEUS and how do they vary monthly and interannually?
- Does the wildfire climatology change for wildfire threat days as compared to actual wildfire days?
- What are the most common synoptic weather patterns associated with wildfires over the NEUS, and how do these weather patterns evolve?
- What is the origin of the dry air that enters the planetary boundary layer for these events?
- What impact do the Appalachian Mountains have on the criteria for fire weather?

Chapter 2 - Data and Methods

a. *Fire weather climatology over the Northeast U.S.*

The fire weather climatology over the NEUS was constructed using actual wildfire days, which consists of 155 major (>100 acres burned) wildfires across the NEUS from January 1999 to December 2009 (Fig. 2.1). The wildfire data were obtained through the Northeast Interagency Coordination Center (NICC) and the Pennsylvania Bureau of Forestry. Since topography, terrain, population, and land surface characteristics are key factors for wildfires, the NEUS was divided into two subregions for this study. Region 1 encompasses much of the higher elevations of the NEUS (Fig. 2.1), while the lee of the Appalachians and most of the coastal plain make up region 2, which includes many of the more urbanized areas. When identifying the days for the actual wildfire, multiple wildfires that occurred for a region on a particular day were only counted once; therefore, the 155 wildfires occurred on 42 separate days in region 1 and 73 in region 2.

The Yarnal (1993) synoptic classification system was used to determine the large scale pressure patterns at the surface associated with the actual wildfire days (Table 2.1). Yarnal identified eight different types of surface pressure patterns over the NEUS. Figure 2.2 shows examples of five Yarnal synoptic types used for this study. The “pre-high” synoptic type occurs when surface high pressure builds southeastward over the NEUS (Fig. 2.2a), which typically occurs after the passage of a cold front. With the surface high centered to the northwest of the NEUS there is usually northwesterly flow. For the “extended high” (Fig. 2.2b), the center of surface high pressure is directly over the NEUS, with light winds across the region. The “back of high” pattern has the center of the high located just to the east of the East Coast (Fig. 2.2c),

which allows for southwesterly flow over the NEUS region. With “high to the south” (Fig. 2.2d), there is also typically a corresponding area of lower pressure to the north, with surface westerly flow between the two pressure centers. On the other hand, a high to the north and a corresponding low to the south allows for an easterly flow across the NEUS (Fig. 2.2e). Other synoptic patterns from the Yarnal classification system which aren’t shown are an “elongated low” which is an elongated area of low pressure, covering a relatively large area, sometimes with multiple centers. “Cyclonic with rain” is when the NEUS is under cyclonic flow with rain. “Cold front” is when a cold front moves through. Finally, “trough” (not part of the Yarnal classification system) is when there is an elongated region of relatively low atmospheric pressure at the surface that is not associated with a cold front.

The National Centers for Environmental Prediction (NCEP) surface synoptic weather maps for 1200 UTC available from the University of Washington (http://www.atmos.washington.edu/data/vmaproom/varchive.cgi) were manually inspected to determine the Yarnal classification of each actual wildfire case in the dataset. If there were missing images from the University of Washington web site, then the analyses from other web sites, such as the Storm Prediction Center (http://www.spc.noaa.gov/obswx/maps/), Hydrometeorological Prediction Center (http://www.hpc.ncep.noaa.gov/html/sfc_archive.shtml), and Plymouth State (http://vortex.plymouth.edu/u-make.html) were used.

b. *Synoptic flow classification climatology*

The North American Regional Reanalysis (NARR; Mesinger et al. 2006) was used to composite the large-scale flow evolution and other meteorological variables for the actual wildfire events. Spatial composites were created for regions 1 and 2 separately using the actual fires dates. Since wildfire start times for many fires were not available, daily composites were created using 3 hourly NARR files from 0000 UTC to 2100 UTC on the date the fire was reported for MSLP and 500 hPa heights. A daily composite of RH and lower level winds would give a false sense of what these conditions were really like during the start of the fire, since these values vary greatly diurnally. Therefore, the 2100 UTC NARR files were used to composite 2-m RH and 925 hPa winds on the date the fire was reported, since this is typically the warmest and driest time of day. For region 1, a composite average using all fire dates for all the states tended to smooth the different fire weather patterns from west to east, so PA was not included in the region 1 NARR composites.

d. *Trajectory Analysis*

The Hybrid Single-Particle Lagrangian Integrated Trajectory (HYSPLIT) model (Draxler and Rolph, 2003) was used to determine the origin of the air near the top of the boundary layer (~850hPa). HYSPLIT computes three-dimensional parcel trajectories using the NARR reanalysis available every 6 h (Mesinger et al. 2006). Backward trajectories at the surface were calculated for 48 h prior to 2100 UTC on the date of each actual wildfire, since this is typically the warmest and driest time of day. Average height, temperature, and RH were calculated for the common synoptic patterns to affect the NEUS during major wildfires.

e. *Impact of Terrain*

The Weather and Research Forecasting (WRF V3.1) model was used to investigate the affects of terrain for a representative case; 7-8 April 2010 event, which was an anomalously warm and dry date in the spring with a westerly component at low levels. Temperatures in New York City and surrounding suburbs of northeast New Jersey are typically around 14 ºC in early April. On this date however, temperatures ranged from 30°C to 35ºC (National Weather Service, New York City 2011). A nested grid model was created, with a 32-km outer grid, 12-km middle grid, and 4-km inner grid. Separate simulations were developed and integrated 24 h beginning 0000 UTC on 7 April 2010. The North American Model (NAM) at 40 km horizontal grid

spacing was used for WRF initial and boundary conditions, and the WRF was set up with 28 vertical levels (testing was done with 38 vertical levels, but proved to make little difference). A control simulation was identified by running the WRF model using various planetary boundary layer schemes; the Mellor-Yamada-Janjic (MYJ), Medium Range Forecast (MRF), and the Yonsei (YSU) (Skamarock et al. 2005) and comparing each run against Automated Surface Observing System (ASOS) observations of 2-m temperature, 2-m RH, 10-m wind, and MSLP archived at the Plymouth State University (Plymouth State University 2011) across the NEUS for 7 April 2010 at 2100 UTC. Also, model soundings were compared to observed soundings at 1200 UTC on 7 April 2010 as well as 0000 UTC on 8 April 2010 at the upper air sites at Albany (ALB) and Upton (OKX). The simulation that most closely matched the observations was chosen for additional investigation. Simulations employing the MRF PBL scheme reproduced the placement and intensity of the warm and dry air along region 2 better than those using other PBL schemes. The simulation with the MRF PBL scheme was then tested using two different soil moisture analyses:

1) With the MRF PBL, NAM initial conditions, and Global Forecast System (GFS) soil moisture,
2) With the MRF PBL, GFS initial conditions, and NAM soil moisture.

These simulations were compared with the previous MRF PBL scheme simulation which used the NAM initial conditions and NAM soil moisture, as well as with the observations. The original MRF simulation still exhibited better agreement with observations. Finally, another simulation was developed using the MRF PBL scheme but with no land surface model instead of the Noah land surface model (Skamarock et al. 2005) used in the original simulations. The original MRF simulation was still found to agree most closely with observations and was therefore identified as the control simulation. A separate experimental case was then run using

the same physics as the control simulation, except the Appalachian terrain was removed (elevation was set to sea level from the Midwest to the East coast), in order to test the impact of the terrain. The control run (MRF) and experimental run (NO_TER) were then compared.

Chapter 3 – Results

a. Actual wildfire climatology

Figure 2.1 shows the spatial distribution of the 155 actual wildfire events from 1999-2009 across regions 1 and 2 of the NEUS. About 61% (96 out of 155) of all actual wildfires occur along the coastal plain in region 2, while 39% occur in region 1. Thus, region 2 has ~0.37 fires per 1000 square kilometer for the 11 year period, while region 1 has ~0.20 fires per 1000 square km. Wildfires are clustered in MA, portions of southwest CT westward to the Lower Hudson Valley in NY, the Pine Barrens of southern NJ in region 2, and in central and northeastern PA in region 1. These areas in region 2 coincide with heavily populated forested regions of the NEUS (figure 1.1).

Figure 3.1 shows the ignition source of the wildfire and the acres burned by those wildfires in the NEUS, which was compiled from data received from the NICC. Although 23% of all acres burned by major wildfires from 1999-2009 were caused by aircraft, this total was due to one event (15550 acres) that occurred on 15 May 2007 in the southern Pine Barrens near Barnegat, NJ. Humans are the main cause for wildfires, with approximately 71% of all events in the NEUS caused by humans. Lightning represents only a small (~0.8% of all acres burned, or ~1.9% of all events) fraction, since the NEUS does not typically experience dry thunderstorms, which are responsible for many of the wildfires that occur in the western US (Rorig and Ferguson 2002).

Figure 3.2 shows the annual percentage of actual wildfire events that occurred from 1999-2009 for regions 1 and 2. The wildfire frequency in region 1 peaks in 2006, with ~24% (10 fires) of the 42 fires in the climatology occurring that year. All 10 wildfires in region 1 in 2006 occurred in the spring (March, April, and May), and 6 (60%) of the wildfires occurred during May alone (not shown). 2002 and 2005 were also active years for wildfires in region 1. There were 7 wildfires in 2002, with 4 of the 7 wildfires (~57%) occurring during the spring (3 of the 4 in April), while the other 3 (~43%) occurred in the summer (June, July, and Augst). In 2005, there were 8 wildfires to affect region 1, with 6 wildfires during April and May. Wildfire frequency in region 2 peaks in 1999, with 22 out of 73 (~30%) occurring in this year, and 10 of these 22 wildfires (45%) during the spring (7 in April).

The average temperature and precipitation for the NEUS was obtained from NCDC (Enloe 2011) to determine whether there were any anomalies. For temperature for region 1, all seasons that had a relatively high number of wildfires (spring 2002, summer 2002, spring 2005, and spring 2006 for region 1) had a warmer than normal season by an average of ~0.78°C. For individual months, only 1 out of 5 months was cooler than normal by 2.4°C (May 2005). The other months (April and August 2002, April 2005 and May 2006) were warmer than normal by ~1.1°C. Active seasons and months are usually associated with a positive temperature anomaly (even though May 2005 was much cooler than normal, the spring that year was above normal by ~1.2°C). For precipitation for region 1, 2 out of 4 seasons that had a relatively high number of wildfires were wetter than normal by an average of ~118% (spring 2002 and spring 2005). The 2 seasons in region 1 that were drier than normal (summer 2002 and spring 2006) were drier by an average of ~93%. For individual months, 3 out of 5 months (April 2002, April 2005, and May 2006) that were active saw above normal precipitation by an average of ~131%. The 2 drier than

normal months (August 2002 and May 2005) were drier than normal by ~73%. This suggests that during some active wildfire seasons in region 1, precipitation may not play a key role. Wildfires can occur just a day or 2 after a significant rain event, since the warm temperatures in the spring and summer dry out the fuels quickly.

For region 2, the spring and summer of 1999 were both above average by 0.7°C and 1.0°C respectively. July 1999 temperature was also above average by 1.6°C. These above average temperatures were associated with below normal precipitation, with precipitation that was 88% and 75% of normal respectively, while July was 78% of normal. Region 2 seems to need both above normal temperatures and below normal precipitation during active years.

Some wildfire years can be unusually dry given the U.S. Drought Monitor archive (National Drought Mitigation Center 2011). May 2006 had abnormally dry conditions (D0, which means the area is experiencing abnormally dry conditions. The area may be going in to a drought with short term dryness and a reduction in planting, growth of crops or pastures. The area may be coming out of a drought where there are still some water deficits and crops and pastures have not fully recovered) (National Drought Mitigation Center 2011) over portions of the NEUS, mainly across PA, where moderate drought conditions (D1, which means there is a moderate drought in existence. Some damage to crops and pastures are noted; low levels in streams and reservoirs are observed. There are also water shortages developing or occurring and voluntary water use restrictions are requested) (National Drought Mitigation Center 2011) were observed in extreme western sections (Fig. 3.3). About 31% of the major wildfires that occurred in 2006 occurred in PA in the month of May, and of all the fires that occurred in May, 62.5% of them occurred in PA (not shown). In 2002, abnormally dry to severe drought (D2, which means severe drought is occurring. Crop or pasture losses are likely; water shortages are common and

water restrictions are imposed) (National Drought Mitigation Center 2011) conditions occurred over some portion of region 1 from 5 March, through 27 August, mainly in PA and ME (not shown). In 2005, abnormally dry to moderate drought conditions occurred over portions of region 1 from 19 April to 30 August, during which there were 4 wildfires (not shown). So, although some major wildfires in region 1 seemed to have occurred during times that the NEUS as a whole saw above normal precipitation, there were smaller areas of the NEUS that saw abnormally dry conditions given the U.S. Drought Monitor.

T-tests were performed on the spring and summer seasons of the active years (1999, 2002, 2005, and 2006) and inactive years (all other years) for the entire NEUS. Both precipitation and temperature were tested to see if there was any difference between the active years and inactive years. Four t-tests were conducted; spring temperatures and precipitation and summer temperatures and precipitation. The result was that neither precipitation nor temperature were significantly different in the active years than in the inactive years. So, although the active years were associated with some above normal temperatures and below normal precipitation, they were not statistically different than the inactive years.

Investigating the monthly distribution of wildfire events will determine when wildfires are most common for the NEUS (Fig. 3.4). There is a peak in actual wildfire events in April in both regions, with ~45% and ~34% of the fires occurring in this month in regions 1 and 2, respectively. April and May comprise ~76% and ~53% of the fires occurring in regions 1 and 2, respectively. During early to mid spring, the vegetation across the NEUS has not fully greened up, thus there are still dead leaves and twigs on the forest floor. This dead vegetation cannot retain water as well as living plants, and even after a period of significant rainfall the dead vegetation dries out rapidly. Li et al. (2010) concluded that from 2001 through 2007 the green

up onset date for latitudes between 40°N and 45°N (southern sections of the NEUS) is between April 10th and 20th, meaning that much of the NEUS is still not green after about the first 2 weeks in April. Additionally, solar radiation and temperatures increase, which allows the fuels to dry out quicker (Parr et al. 2005, Kassomenos 2010).

In contrast, during the summer (JJA) only ~10% of the actual wildfires occur in region 1 and ~22% in region 2 (Fig. 3.4). During summer the live vegetation typically holds abundant moisture, which prevents the fuels from igniting easily, and the relatively humid conditions in summer also are less favorable for wildfires. During the winter (DJF) there is little or no fire activity (~0% for region 1 and ~3% for region 2), since the ground is cool, damp, and snow covered on average.

b. Synoptic flow classification climatology

Figure 3.5 shows the climatology of synoptic flow patterns (defined in Table 2.1) for the actual wildfire days using the Yarnal classification scheme. The pre-high (PH), back of high (BH), and extended high (EH) types together account for ~78% of the wildfire events in region 1 and ~77% in region 2. The EH is the most common synoptic type in region 1 (~45% of all events), while the PH type is most common in region 2 (~30% of all cases). The combination of cold fronts (CF), elongated low (EL), high to the south (HS), surface trough and high to the north (HN) together account for ~21% and 23% of the fire events for regions 1 and 2, respectively. A

CF is often associated with precipitation, so it has a relatively low percentage (~10% of all cases in region 1 and 14% region 2). The EL type is also often associated with precipitation, and thus there were only a few wildfires in both regions associated with this synoptic type. Meanwhile, a HN (0% in both regions 1 and 2) allows an easterly flow to develop, which advects cool and moist marine air from the Atlantic Ocean towards the NEUS.

Figure 3.6 shows the monthly percentage for each synoptic type for the actual fire days in region 1. The EH type is more common (occurs 12% more than the next most common synoptic type, CF, and 14% more than the other synoptic types that occur, PH and BH) than all the other synoptic types during the peak of fire season (~21% in April), and occurred 19% of the time in May. Major wildfires with CFs (~10%) only occurred in April in region 1, while trough events (~5%) only occurred in May. EH and BH are the dominant synoptic types associated with major wildfires in July and August in region 1 (~2% for both synoptic types in July, and 5% for BH and 0% for EH in August).

For region 2 (Fig. 3.7), although the PH type is the most common pattern overall (~27%), it is not the most common type in any individual month. Rather, during the peak of fire season in April, the PH is similar to BH (~10%), while the EH is the dominant type in May (~8%). Wildfire activity associated with CFs is mostly in April, but it also occurs in the months of May, June, July, and October.

Overall, the EH type is more common in region 1 (45% of all wildfire days) than region 2 (23% of all wildfire days), especially during the peak of fire season. About 45% of EHs were multi-day (2 days or more) events (not shown). As noted by Barriopedro et al. (2005), a blocking flow pattern is most frequent over the NEUS during the spring months, which is the most

common time to see an extended high type pattern associated with wildfire activity. There were 19 EH events for region 1. The composite for these events (not shown) shows a well defined trough off the east coast, and a well defined ridge over the eastern third of the U.S., with the ridge axis extending from the eastern Great Lakes to the central Gulf Coast. There is some minor troughing over the mid-West and central Plains states, but it does not resemble a classic blocking pattern. Inspection of each individual EH case revealed 12 out of 19 (63%) cases had a blocked pattern at 500 hPa, a majority of which were the omega type blocking pattern. This blocking pattern allows for an extended period of drying and warming over higher terrain of the NEUS (region 1). Wildfires may be less common for EH events in region 2, since the inland warming and weak wind speeds underneath the surface high allow for sea breeze boundaries to develop over coastal sections during this time of year (Novak and Colle 2006), which allows cooler, moist air to advect into the region from the ocean, thus decreasing the chance for wildfires.

c. *Synoptic composites*

Spatial composites were created using the NARR data as described in section 2 for actual wildfire days in regions 1 and 2 separately. At 48 h prior (t-48) to a fire event in region 1 (Fig. 3.8a), there is a surface high pressure over the eastern Great Lakes, while there is a weak surface

low just east of the mid-Atlantic states. The 925 hPa wind directions range from westerly and northwesterly over southern and western sections of the NEUS to north-northwesterly and northerly over northern and eastern sections of the NEUS. Wind speeds are 5 m s^{-1} and below. Potential temperatures range from between 288K–293 K in extreme southern PA to 278K–283 K in northern NEUS, with a majority of the NEUS between 283K–288K. On the day of the event (t=0) in region 1 (fig. 3.8b), the center of the surface high moves south, located just south of the NEUS, over West Virginia and Virginia, and is similar to the EH pattern in the Yarnal classification, while the surface low off the mid-Atlantic states has moved slightly east. The 925 hPa wind speeds over the NEUS are generally northwesterly, with some westerly and southwesterly winds in southwest PA, and northerly winds along southern coastal sections. Wind speeds are still 5 m s^{-1} or less. Warmer potential temperatures have advected northeast slightly and range between 283K-293K across the NEUS.

There is a broad ridge at 500 hPa (fig. 3.9a) at t-48, from the western Great Lakes south-southwestward to Texas. Winds at this level are northwesterly at about 10 m s^{-1}. The NEUS lies between two jet streaks at 300 hPa, one well off the NEUS coast oriented southwest to northeast, situated just east of the 500 hPa trough axis that is over the western Atlantic with a jet core of 25 m s^{-1} to 27 m s^{-1}. The other jet streak is north of the western Great Lakes in southern Canada oriented west to east with a core of 23 m s^{-1} to 25 m s^{-1}. Winds speeds over the NEUS are between 15 m s^{-1} and 17 m s^{-1}. At t=0 (fig 3.9b), the 500-hPa ridge axis has moved to the central and eastern Great Lakes and has amplified, while the upper level trough is still situated ~750 km east the U.S. East coast and has also amplified. Winds at this level remain northwesterly at about 10 m s^{-1}. The jet off the NEUS coast has pushed farther east, while the jet over southern Canada has moved southeast and is situated north of the Central Great Lakes

region over southern Hudson Bay. The core has strengthened to between than 27 and 29 m s^{-1}. The NEUS lies in a somewhat favorable area for subsidence to occur. It is a well known fact that within jet circulations, subsidence occurs over the right exit regions of upper level jets. The NEUS lies near this position, especially northern portions of the NEUS. Subsidence is observed over the entire NEUS in a plot of average 600 hPa to 300 hPa vertical velocity for region 1 at t0, with some enhanced sinking occurring over central NY and northern VT and NH (fig. 3.10).

Figure 3.11a shows the composite 2-m RH, 925 hPa wind, and 2-m temperature for region 1 at t-48 and t=0 (fig. 3.11b) the day of the event. The lowest RHs (45-55%) are from the majority of PA and stretches east and northeast into all of NJ, New York City, the Lower Hudson Valley, western, northern, and northwest CT, northern RI, western MA, and southern NH at t-48h. 2-m temperatures generally range from 11°C – 13°C in ME, to 18°C in extreme southern and southwestern PA. There is a temperature gradient along the immediate coast where the relatively cool waters meet the warm inland temperatures, and temperatures here are as low as 9°C. At t=0 in region 1 (Fig. 3.11b), the RHs decrease to less than 45% across extreme southern NJ and extreme southern PA. A larger area of 45%-50% RH values exists over central and eastern PA and most of NJ, which extends into southern NY and the lower Hudson Valley. The rest of the NEUS has RH values of between 55%-65%. This composite analysis suggests that these fire events can occur even though the RH values are greater and wind speeds are less than the criteria for a RFW (30% RH and 11.2 m s^{-1} wind speed). However, comparing NARR and the actual surface observations for a few cases, the NARR was too moist by 15-30% (not shown), therefore illustrating the difficulty in obtaining an accurate low-level moisture analysis for these relatively dry fire events. The 2-m temperatures have generally increased 2°C-3°C at t=0, with the warmest air over PA where temperatures range from 18°C-21°C. Northern sections

of the NEUS have warmed to generally between 13°C-15°C, with the immediate coastal sections as low as 11°C.

Figure 3.12a shows a cross section of potential temperature, winds, and vertical velocity along latitude 42.2N at t-48 from longitudes 70.78W to 79.5W. From 73.0W to 70.78W is region 2, and from 73.0W to 79.5W is region 1 and is denoted by the vertical line. There is some instability in the lower levels between 74.5W and 78.5W in region 1 as the 280K isentrope slopes. There is upward motion in the lower levels from just above the surface to around 800 hPa, with maximum upward motion seen at around 75.0W, with values between -0.15 Pa s^{-1} to -0.10 Pa s^{-1}. This upward motion in the lower levels of region 1, and downward motion in region 2 is associated with upsloping and downsloping winds, as the lower levels have enhanced vertical velocities (negative for region 1 and positive for region 2), while at the same time a westerly or northwesterly cross barrier flow exists. There is downward motion associated with synoptic subsidence from 800 hPa to about 300 hPa over region 1. The west to northwest winds at the lower levels veer to the northwest for western portions of region 1 indicating an area of warm advection for extreme western portions of region 1 from 78.0W to 79.0W. At t=0 (fig. 3.12b), the area of instability in the lower levels moves east, between 73.0W and 76.0W with a sloping 285K isentrope, while the upsloping continues in region 1 and downsloping occurs in region 2 in association with negative and positive vertical velocities respectively in the lower levels, and synoptic scale subsidence occurs from about 900 hPa and above.

For region 2 at t-48 h (Fig. 3.13a), there is an area of surface high pressure near western North Carolina and eastern Tennessee, and a surface trough just off the east coast, with the trough axis extending from 500 km to 650 km east of the coast of Georgia, northeast to between 800 km and 900 km east of Virginia. The 925 hPa winds are generally northwesterly at about 5

m s^{-1} or less, and potential temperatures range between 283K-288K over southern NEUS in PA to 273K-278K over extreme northern NEUS in northern ME. A majority of the NEUS is between 278K-283K. At t=0 (Fig. 3.13b), the surface high pressure has remained nearly stationary with a slight increase to 1022 hPa. As a result, a PH type pattern is established across the NEUS, with westerly or west-northwesterly 925 hPa flow across the NEUS. Wind speeds are still at 5 m s^{-1} or less with nearly the same potential temperature range as t-48.

In the upper levels, at t-48 (Fig 3.14a), there is a broad 500-hPa ridge over the central portions of the U.S., while an upper-level trough is located ~750 km east of the East coast. 500 hPa winds are northwesterly at 20 m s^{-1}. At 300 hPa, there is a jet oriented east to west from south central Canada and the Northern Plains to southeastern Canada, with wind speeds of 21 m s^{-1} to 23 m s^{-1}. By t=0 (Fig. 3.14b), the upper level pattern is similar to 48 h earlier, with wind speeds of 15 m s^{-1} at 500 hPa. At 300 hPa, there is a jet streak over southeastern Canada oriented northwest to southeast, with the a jet core of between 25 m $s^{-1}$and 27 m s^{-1} just north of the eastern and central Great Lakes region and south of the Hudson Bay. As with region 1, subsidence is observed over much of the NEUS in plots of 600 hPa to 300 hPa averaged vertical velocity for region 2 at t=0 (figure 3.15), with some enhancements over northern VT, NH, and ME, with no real enhancements noted for portions of region 2. It cannot be made clear from this plot whether the jet is enhancing the subsidence over this region as gravity waves may be playing a part in enhancing the vertical velocities (seen in the coupling of sinking and rising air over the higher terrain, particularly over WV and VA).

The lowest surface RHs (45%-50%) occur over extreme southern PA, but a larger portion of low RH (50%-55%) exists over the coastal plain (Fig 3.16), from southern NH to New Jersey at. This region of lower RHs corresponds to the cluster of past wildfires (Fig. 2.1). The location

of the lowest RH for t-48 (fig. 3.16a) and t=0 (fig. 3.16b) is east of the Appalachian Mountains. The westerly component favors downslope drying over the coastal plain, with relatively strong low level subsidence noted from the surface to about 700 hPa (values of +0.09 Pa/s to +0.12 Pa/s) in cross sectional composite at t-48 (fig. 3.17a). Synoptic scale subsidence exists above 700 hPa with lower values of positive vertical velocity (values of 0 Pa/s to +0.09 Pa/s). Once again, lift is seen in association with cross barrier westerly flow leading to upsloping in region 1 with negative values of vertical velocity. Much of the same is seen at t=0 (fig. 3.17b)

In order to gain an understanding of where the subsidence is coming from in a quasi-geostrophic sense, the Sutcliffe-Trenberth form of the quasi-geostrophic omega equation (Trenberth 1992) was used. This equation states that anticyclonic vorticity advection by the thermal wind is associated with downward motion (term A in the Sutcliffe-Trenberth QG equation). Figure 3.18 shows the 600 hPa to 300 hPa thermal wind and term A (vorticity term) composite for regions 1 and 2 for t=0. Both regions show anticyclonic vorticity over the NEUS, and more being advected in by the northwesterly direction of the thermal wind crossing over the gradient of anticyclonic vorticity in a region to the to the northwest of the NEUS. The values for region 1 are stronger as compared to region 2

Figure 3.19 shows a box and whisker plot of the RH (Fig. 3.19a) and wind speed (Fig. 3.16b) for both regions 1 and 2 at t=0. The white line is the areal mean. The mean areal average for region 1 is ~60%, while for region 2, it is ~63%. For wind speed, the areal average for region 1 is 5.7 m s^{-1}, while for region 2 it is 6.3 m s^{-1}. The whiskers show the minimum and maximum areal average values observed on the wildfire dates for each region. While both regions share the same minimum areal average value RH of ~43%, major wildfires in region 2 have occurred at much higher areal average RH values than region 1 (~89% and 74% respectively). Areal

average wind speed minimum and maximum values seem to be similar for regions 1 and 2, with minimum values of 0.23 m s^{-1} and 0.73 m s^{-1} and maximum values of 14.1 m s^{-1} and 15.42 m s^{-1} respectively. The standard deviation for region 1 for RH is 8.5 and for region 2 is 9.5, so the maximum RH value of 89% is ~2.7 standard deviations from the mean, while the 74% maximum value in region 1 is 1.7 standard deviations away. The minimum RH values are 2.1 for region 2 and 2.0 standard deviations for region 1. This data suggests that wildfires occur in region 2 at a larger range of RH. The standard deviations for wind speed are much closer for both regions, with a standard deviation of 3.0 in region 1 and 2.8 in region 2, indicating that wind speed does not differ much between the 2 regions for wildfires.

d. *Trajectory analysis*

The synoptic composites show that wildfires can occur for different surface pressure patterns over the NEUS. High pressure is the result of subsidence, and subsidence creates warmer and drier conditions. In order to determine the origin of the subsidence and dry air on the large scale, back trajectories starting later in the afternoon at 2100 UTC (start times of fires are unavailable so 2100 UTC was used, since this is typically the warmest and driest time of the day) were run to 48 hours prior, starting at 1500 m above sea level (this height was chosen because it has been shown that air from upper levels of the atmosphere descend to the midlevels [Charney 2009]). Since subsidence is sinking air, i.e., downward vertical motion, the average

height along 6 different trajectories (Fig. 3.20) of the 3 major synoptic types to affect the NEUS during wildfire events (PH, EH, BH) were calculated. Figure 3.21 shows the average of all 28 PH heights along the six different trajectories. Six trajectories were chosen to gain a good enough spread across the NEUS, while at the same time it is a low enough number of trajectories to easily see each trajectory. Figure 3.20 shows the location of the start points of the trajectories. #1 is southern NJ, #2 is central PA, #3 is the lower Hudson Valley in southern NY, #4 is in CT, #5 is in MA, and #6 is in VT. These points were chosen to be at or near the cluster of major fires discussed earlier. Because PA was the only state that had a cluster of large wildfire activity in region 1, VT was chosen randomly as another point for region 1, otherwise there would only be 1 point representing region 1. On average, during a PH event, trajectories at 1500 m above ground level start between 2000 and 3500 meters above ground 48 hours prior (fig. 3.21), with 4 out of 6 trajectories starting between 3000 and 3500 meters. This corresponds to about 500 meters to 2000 meters of descent. Trajectory #2 shows the most subsidence, starting out at ~3350 m on average 48 hours prior, while trajectory #6 shows the least subsidence, only starting out at ~2100m. Figure 3.22 shows the average of all 32 EH heights, with all the trajectories starting out 48 hours prior with heights ranging from 2250m–2750m. Trajectory #2 shows the most subsidence as it has the highest starting point (~2700m), while trajectory #6 has the lowest (~2350m). Figure 3.23 shows the average of all 24 BH events. The trajectories start out between 1750m-2250m 48 hours prior to the event. All but 1 trajectory (#1) fall below 1500m starting 27 hours prior (1800 UTC on day 2, trajectory#6) and then rise to 1500m to the start of the trajectory on 2100 UTC on day 1. This suggests that from 27h to 18h prior to a wildfire event in BH cases there is some rising motion occurring. Out of all 3 synoptic types, PH seems to subside the most, while BH subsides the least, and even shows some lift just before the event.

Figure 3.24 shows the average RH along the 6 trajectories for the PH type. RHs start out between 45%-60% 48h prior to the events. The largest decrease in RH occur with trajectories 1, 3, 4, and 5. They start out between 50%-55% and end at ~35%, which is a 15%-20% drop in RH. The largest drop off in RH seems to occur between 2100 UTC on day 3 to 0300 UTC on day 1, and levels off thereafter. Trajectory 6 shows the least drop off in RH (~12% decrease). Figure 3.25 shows the average RH along the 6 trajectories for the EH type. RHs start out between 38%-49% and end between 35% and 42%. While PH shows a steady decrease throughout much of the individual trajectories (with the exception of some minor increases), EH shows a steady increase in RH beginning 1800 UTC on day 2 and ending on 1200 UTC on day 1 before dropping off again through 1800 UTC on day 1. As a whole, the BH type shows little change in RH from the beginning to the end of the trajectories (fig. 3.26). Trajectories start out and end between 40%-50%. Trajectories 1, 2, 3, and 6 show slight increases, while 4 and 5 show slight decreases. Out of the 3 synoptic types, PH shows the most decrease in RH, while BH generally shows a slight increase.

Figure 3.27 shows the average temperature along the 6 trajectories for the PH type. Trajectories start out between -17°C to -9°C 48h prior and end between -4°C and +4°C. Five out of the six trajectories show and increase in temperature of between 15°C and 20 °C, while one trajectory (#6) shows only ~6°C increase. For the EH type (fig. 3.28), the temperature curves for all 6 trajectories are very similar. Temperatures start out between -5°C and 0°C and increase to +5°C and +10°C, leading to a 10°C increase in temperature. The BH temperature curve (fig.3.29) for the 6 trajectories are also very similar. Temperatures start out between +5°C and +10°C and end between +10°C and +15°C. This corresponds to ~5°C increase. Comparing the 3 synoptic types, PH shows the greatest increase in temperature, but the actual temperature

values are the lowest. BH shows the least temperature increase, but the actual temperature values are the highest. Finally, EH is in the middle of the other two.

For the PH type, trajectory 6 is an outlier, showing the lowest decrease in height, the lowest decrease in RH, and the lowest increase in temperature. Trajectory 6 is in region 1 in VT. The other region 1 trajectory (#2 in PA) shows one of the highest decreases in height and temperature. Meanwhile, the trajectories in region 2 (1, 3, 4 and 5) show similar decreases in altitude, RH, and increases in temperature compared to each other. This may suggest that the subsidence, decrease in RH, and increase in temperature may be more varied in region 1 than in region 2 during a PH type event, which is the predominant type to affect region 2. In the other synoptic types, trajectory 6 is less of an outlier, indicating that the same values are less varied for these synoptic types, which includes EH (the predominant type to affect region 1).

e. *Impact of the Appalachian Terrain*

A number of studies across the western U.S. have shown that downslope flow helps to prime the fuels for the ignition and spread of wildfires through adiabatic warming (Raphael 2003, Radtke et al. 1982), but there have been no notable studies of the terrain's effect on temperature and RH over the NEUS. The downslope process can have a great impact on wildfire threat. The question is how much does the higher terrain of the Appalachians increase the potential for wildfire across the lower altitude coastal Plain of the NEUS during a period of

westerly cross barrier flow? The above Hysplit trajectories cannot resolve the terrain effects, so a higher resolution modeling approach is needed.

The 7-8 April 2010 case was chosen due to the previously discussed anomalously warm and dry conditions along the coastal plain. This was a BH type event. This synoptic type was chosen because the southwesterly flow does lead to some downsloping. Figure 3.30 shows a topographical map of much of the Eastern U.S. seaboard. The darker colors are the higher elevations, with areas above 914 meters (3000 ft) in black. The highest terrain for the Eastern U.S. are in portions of West Virginia (WV), Virginia (VA), and North Carolina (NC). Arrows show a southwesterly flow. A southwesterly flow would downslope into the lee of the higher elevations in this area, and then advect into southern portions of the NEUS, such as southeastern PA, NJ, the New York metro area, Lower Hudson Valley, Long Island, and CT and RI. The higher elevations in PA and NY would most likely downslope and advect into MA, and southern portions of VT, NH, and ME. More downsloping would occur over WV, VA, and NC, as the mountains here are higher than in the NEUS. The extremely high temperatures and low RHs provided an opportunity to study the impacts of downslope on fire weather for this highly populated area. There is more of a societal impact to region 2 than region1 due to its higher population and population density. Although PH is the more frequent synoptic type to affect region 2, this study has shown that it was not the most common type during April – the peak of wildfire season, nor was it the more common type during the wildfire season in its entirety – April and May. BH was just as common as PH in April and more common than PH in May. Finally, studying the impact of terrain on the NEUS by setting the higher terrain to sea level and observing its effects on the fire weather parameters has never been tested in this way.

A verification of the control run at 2100 UTC on 7 April 2010 (this time was chosen, because it is typically the warmest, driest, and windiest part of the day - prime conditions for the start and spread of wildfires) is presented and then followed by its comparison to the experimental run. In the control run (fig. 3.31a), a large area of warm air of 27°C+ lies along the coastal plain, from MA southeast into the mid-Atlantic states such as Virginia (VA), Delaware (DE), central and eastern Maryland (MD), and northeast North Carolina (NC). The warmest of the air lies over the Boston metro area in eastern MA, into CT, northern RI, southern portions of the Lower Hudson Valley, the New York City metro area, as well as eastern DE, VA, and northeast NC. This coincides with the warmest air in the observations (fig. 3.31b), though the model is too cool as there are many areas of 30°C+ noted over the locations previously mentioned. When testing for the control run, all models were too cool, but the MRF run came the closest to capturing the strength and areal extent of the warm air.

For RH, there is a large area of <30% RH along the coastal plain, in eastern MA, RI, much of CT, extreme southern NY, central and southern NJ, and southeast PA, as well as DE, central MD, eastern VA and northeast NC (fig. 3.32a). This is also where the warmest temperatures are located. Although the driest air is over West Virginia (WV) in the observations (fig. 3.32b) with RH values of <15%, the larger area of <30% is in the same areas previously mentioned. The RH values are too high in the model, but as with temperature, when testing for the control run, all runs were too moist, but the MRF came closest to capturing the driest air and its areal extent.

Wind direction in the control run (fig. 3.32a) are southwesterly from central and southern NEUS into the mid-Atlantic states. Winds shift to the northwest in northern NEUS. Strongest wind speeds are over the same areas as the driest air and warmest temperatures with wind speeds

of 10 m s^{-1}. Winds in the observations (fig.3.33) are generally west to southwesterly over the southern NEUS, with a west or northwesterly direction in the northern NEUS. The strongest wind speeds are also seen in the areas of driest and warmest air in the observations.

Finally, there is a 998 hPa surface low pressure over southern ME in the model (fig. 3.34) which is also seen in the observations (fig. 3.35). A >1020 hPa surface high pressure lies well off the southeast U.S. coast in the western Atlantic in both the model and the observations.

The control vs. experimental run temperatures are compared in figure 3.36. Temperatures in the experimental (fig. 3.36b) run decrease over the coastal plain (region 2) by 1°C to 2ºC. The warmest air in the control run (fig. 3.36a) (over eastern MA, CT, northern Rhode Island, southern portions of the Lower Hudson Valley, and New York City) which were between 28°C and 29ºC are now between 26°C and 27ºC. The large area of 27ºC+ along the coastal plain has decreased to 26°C+.

The control vs. experimental run RH values are compared in figure 3.37. The areal coverage of 20%-30% RH along the coastal plain in eastern MA, RI, much of CT, extreme southern NY, central and southern NJ, and southeast PA, as well as DE, central MD, eastern VA and northeast NC in the control run (fig. 3.37a) is decreased in the experimental run (fig. 3.36b), and is generally limited to the coastal plain of the NEUS with only a few widely scattered pockets in the previously mentioned mid-Atlantic states. Figure 3.38 shows the RH difference (control minus experimental) between the control and experimental. The greatest drops (which denotes an increase in RH in the experimental run) are seen over southern ME and northern NY and VT. The coastal plain sees a drop in RH values between 0%-8%. The higher elevation areas (region 1) actually sees more of a decrease in RH from the control run. RH decreases by at least 4%-8% over western PA, central NY, southern VT, southern NH, and central and southern ME,

with numerous scattered pockets of decreases of 8%-12% and 12%-16%. This is likely due to the fact that the higher terrain has been removed.

In conclusion, the results of the terrain sensitivity study show that in this case of southwesterly flow over the NEUS, the downsloping winds decrease temperatures by 1°C to 2ºC over much of the coastal plain, while RH values drop by 0%-8%. Although results only show minor increases in temperature and minor to moderate decreases in RH, this is only one case, and other case studies may show larger increases in temperature and lager decreases in RH. Back trajectories run up to 72h prior to this event shows (not shown) the origin of the dry air to be over the North Carolina/Tennessee border, and a southwesterly flow advects this air into the NEUS. Downsloping may still be important for this case, but for the southern Appalachians as opposed to the northern Appalachians. A southwesterly flow over the southern Appalachians in western North Carolina and Virginia descends into the coastal plain of eastern North Carolina and Virginia, then continues on its southwesterly flow into the NEUS. This is evident in plots of 900 hPa vertical velocity (not shown). There is an area of subsidence just east of the higher terrain of NC, VA, and WV, coupled with drying and warming at this level (not shown). Observations on 06 April 2010 from 1200 UTC to 2100 UTC (not shown) show an area of low RH developing at the surface over portions of North Carolina and Virginia, which eventually advects into the NEUS. Further study into the terrain effects of the NEUS are important because the larger the increase in temperature and decrease in RH the faster the fuels will dry, putting the area at risk for wildfires (Wagner 1979).

f. *Actual wildfires versus threat days*

The primary goal of this study was to develop an annual and monthly climatology for actual wildfires over the NEUS, but it does not include the large number of days with a wildfire threat. A goal of the fire weather community is to alert the public when there is the *potential* for the ignition and spread of wildfires, which is defined as wildfire threat. Also, meteorological wildfire threat along the East Coast needs to be better understood (Charney et al. 2003; 2006; 2009). Therefore, in this section an abbreviated analysis of wildfire threat days will be shown, so it can be compared with the above actual wildfire days over the NEUS.

The wildfire threat climatology was based on NFDRS ratings, since there were not enough RFWs issued to build a sufficient climatology. The climatology was created using days when 50% or greater of the NEUS had a NFDRS rating of "high" or greater, which was accessed from the Wildland Fire Assessment System (WFAS) database (www.wfas.net). There were 194 days from Jan 1999-Dec 2009 that met this criterion. The WFAS archived NFDRS maps are only available for entire states so it was not possible to subdivide the events into the two regions shown in figure 2.1.

For the annual wildfire threat climatology (Fig. 3.39), there is a peak in 1999 and a secondary peak in 2006, which agrees well with the actual wildfire results (Fig. 3.2). Also, 2007 was one of the least active fire threat years (~2.1%), as well as the least active actual wildfire year for region 2 (~2.4%). This is likely due to the abnormally wet and cool April 2007, which was the 3rd wettest and 25th coldest on record for the NEUS (Enloe 2010).

For the monthly climatology of wildfire threat (Fig. 3.40), there is an increase from January (~6%) to February (~13%). This result is slightly different than actual fires, where there is a significant increase of actual fire activity from March to April (Fig. 3.4). A possible explanation is that NFDRS does not output ratings when there is snow on the ground. This leads to a north-south gradient on the NFDRS wildfire threat map during February and March, where northern sections will have a low or moderate rating, while southern sections will have a high or greater rating. The higher ratings for southern sections are enough to lead to an increasing number of February events when considering the whole NEUS. Just over 30% of all days in February and March had this north-south boundary, and 100% of days with data available were associated with snow in northern NEUS. Also, since humans are the leading cause of wildfires in the NEUS, it stands to reason that although there is an elevated wildfire potential during the colder months of February and March, wildfires do not occur frequently due to a relative lack of human activity.

Chapter 4 – Conclusion

The goal of this study was to develop an annual and monthly climatology for the Northeast U.S. (NEUS) for wildfires. The synoptic pattern in place during these events and their origin and evolution were determined, and the role of downsloping off the Appalachian mountains was addressed. The annual and monthly climatology of wildfire events was summed over the NEUS for actual major wildfire events (> 100 acres). There was a peak in wildfires in 1999 for region 2 (coastal plain), and in 2006 for region 1 (interior Northeast). These years were marked by abnormally warm and dry conditions. The wildfire season over the NEUS is April and May, with the peak occurring in April. This is likely due to the pre-green up period across the NEUS, increasing solar radiation, and the continental high pressure systems that move into the region during this time of year. There is a minimum in wildfire activity in the winter (DJF) due to the cool, damp conditions present during this time of year and the presence of snowpack.

Pre-high (PH), extended high (EH), and back of high (BH) are the 3 common types of high pressure systems to affect the NEUS during wildfire events. PH establishes a flow that is favorable for downsloping, especially across region 2, where PH is most frequent. EH is the most common type in region 1. This is usually a large area of high pressure that can take days to move across the region, and occurs during a time of year when blocking patterns are common for this section of the country. The time it takes to move across the NEUS allows for persistent dry conditions, which permit the fuels to dry. A southwesterly flow is normally established in a BH synoptic type. The westerly component allows for some downslope and therefore dry conditions while the southerly component advects warm air into the NEUS.

Temporal evolution of synoptic plots show the origin of the high pressure systems is from the eastern Great Lakes region for region 1. Over a 48 hour period, this high pressure moves to a position over the NEUS, classifying it as an EH type. For region 2, a PH type is already in place over the NEUS, and is nearly stationary over the 48 hour period with some strengthening noted. Little change is seen in RH values and 925 hPa wind speeds over region 1 when comparing t-48 and t=0. Slight drying occurs in region 1. Of particular interest with these variables is the fact that both variables lie outside the criteria for RFWs for the NEUS. This begs the question "Do RFW criteria need to change for the NEUS?" The NEUS is not subject to the same types of severe meteorological wildfire conditions as the western portions of the U.S., and therefore it is reasonable to assume that the NEUS may be more sensitive to the conditions that allow wildfires to grow because major wildfires occur at higher RH values and lower wind speeds for the NEUS as compared to the West.

HYSPLIT back trajectories show that the PH synoptic type undergoes the most subsidence, the largest decrease in RH, and the largest increase in temperature, while BH undergoes the least subsidence, least decrease (and in some cases an increase) in RH and least increase in temperature. The EH type stands in the middle of these synoptic types. The 850 hPa layer may be important when daytime heating allows for turbulent eddies to form and some of the drier air at this level is transported to the surface. Also, as the air descends from 850hPa, temperatures will increase further, allowing fuels to dry out quicker. This is supported by other studies previously mentioned.

Terrain sensitivity studies show that for one case study, the impact of cross barrier flow over the NEUS shows only a 1°C to 2°C increase in temperatures and a 0%-8% decrease in RH at the coastal plain (region 2). Decreases in the areal extent of the warmest and driest sections

were noted. Further study on different types of downsloping events (this study used a southwesterly flow, different results with westerly and northwesterly flow are likely) are needed to gain a full understanding of the terrains effect on temperature and RH across the NEUS during downsloping events. This will help in fire weather forecasting across the NEUS because fuels are sensitive to changes in temperature and RH.

The results from this study are useful in an operational forecast setting. For example, noting that a PH or EH type synoptic pattern will set up over the NEUS after a period of dry weather would be a signal to forecasters that conditions may be favorable for wildfires to occur. In contrast, an EL, CF, HN, ST pattern will allow forecasters to realize that wildfires will be unlikely to occur. By describing the time of year when that NEUS experiences both wildfire threat and actual wildfires, a forecaster will be better prepared to look for conditions during the peak of wildfire season in April, while still noting that wildfires are possible but not as likely for other months. As noted previously, RFW and FWW conditions vary from region to region, as well as their meanings. For example, in some areas of the country, an RFW means that conditions are favorable to conduct a prescribed burn, while in others an RFW means that there are very unusual conditions and the fire management community must take the proper action to quickly respond to any reports of wildfires. Therefore, understanding the frequency of actual wildfire days and wildfire threat is valuable information for the forecaster.

Criteria for RFWs are determined by the NWS along with representatives from the fire management community (Tim Morrin, NYC National Weather Service, 2011 personal communication). However, these criteria are not necessarily set by a proper understanding of the frequency of high wildfire danger days and actual wildfire days. This begs the question whether RFWs (and FWWs) capture an optimal percentage of high wildfire days or actual wildfire days.

Also, as previously noted, the NEUS is more sensitive to wildfires than the western U.S. i.e., this study has shown that they can start at higher RH values and lower wind speeds than is set for the WFO OKX forecast area. This study could be used to help reevaluate the criteria for RFWs and FWWs.

The information in this study may also be used to differentiate between unusual wildfire weather events and those that are more routine. For example, if there is a high wildfire danger day expected in the month of January, the forecast can mention that this occurs once in ten years.

A simple conceptual model can be constructed with the synoptic composites that were developed to help aid forecasters. For region 1 (fig. 3.41a), an extended high type is in place, with the center of the high located near the spine of the Appalachians, generally south of the NEUS, but extends into southern portions of the NEUS. A weak surface low pressure system is located well off the East coast in the western Atlantic. At 500 hPa, there is a ridge over the Great Lakes region, the axis of which extends into the Gulf States, with a trough of low pressure to the east of the surface low (generally located between the surface high and surface low). Finally, at 300 hPa, there is a jet streak over southeastern Canada, just north of the Great Lakes oriented west to east. For region 2 (fig. 3.41b), there is a surface high located at or just to the west of the spine of the Appalachians. Since the center of the high is still to the southwest, high pressure is still building into the region, and this is classified as pre-high type. A surface trough is well off the East coast in Western Atlantic. The 500 hPa features are much flatter than in region 1, with a broad ridge over the Great Lakes and mid-West region. At 300 hPa, there is a jet streak over southeastern Canada and the northern and eastern Great Lakes, extending into northern portions of the NEUS. This jet is oriented northwest to southeast.

Tables

YARNAL CLASSIFICATION	DESCRIPTION
Extended high (EH)	Covers a large area, sometimes with multiple centers.
Pre-high (PH)	High building in after the passage of the cold front. Centered to the west or northwest of the Northeast U.S.
Back of high (BH)	Western side of high pressure system. High is usually centered off the East Coast.
High to the south (HS)	Center of high pressure to the south, with low pressure to the north. Leads to westerly winds.
High to the north (HN)	Center of high pressure to the north, with low pressure to the south. Leads to easterly winds.
Elongated low (EL)	An elongated area of low pressure, covering a relatively large area, sometimes with multiple centers.
Cyclonic with rain (RC)	Area is under cyclonic flow with rain.
Cold front (CF)	Cold front moving through.
Trough	An elongated region of relatively low atmospheric pressure at the surface that is not associated with a cold front (not part of the Yarnal classification)

Table 2.1. Yarnal synoptic classification scheme.

Figures

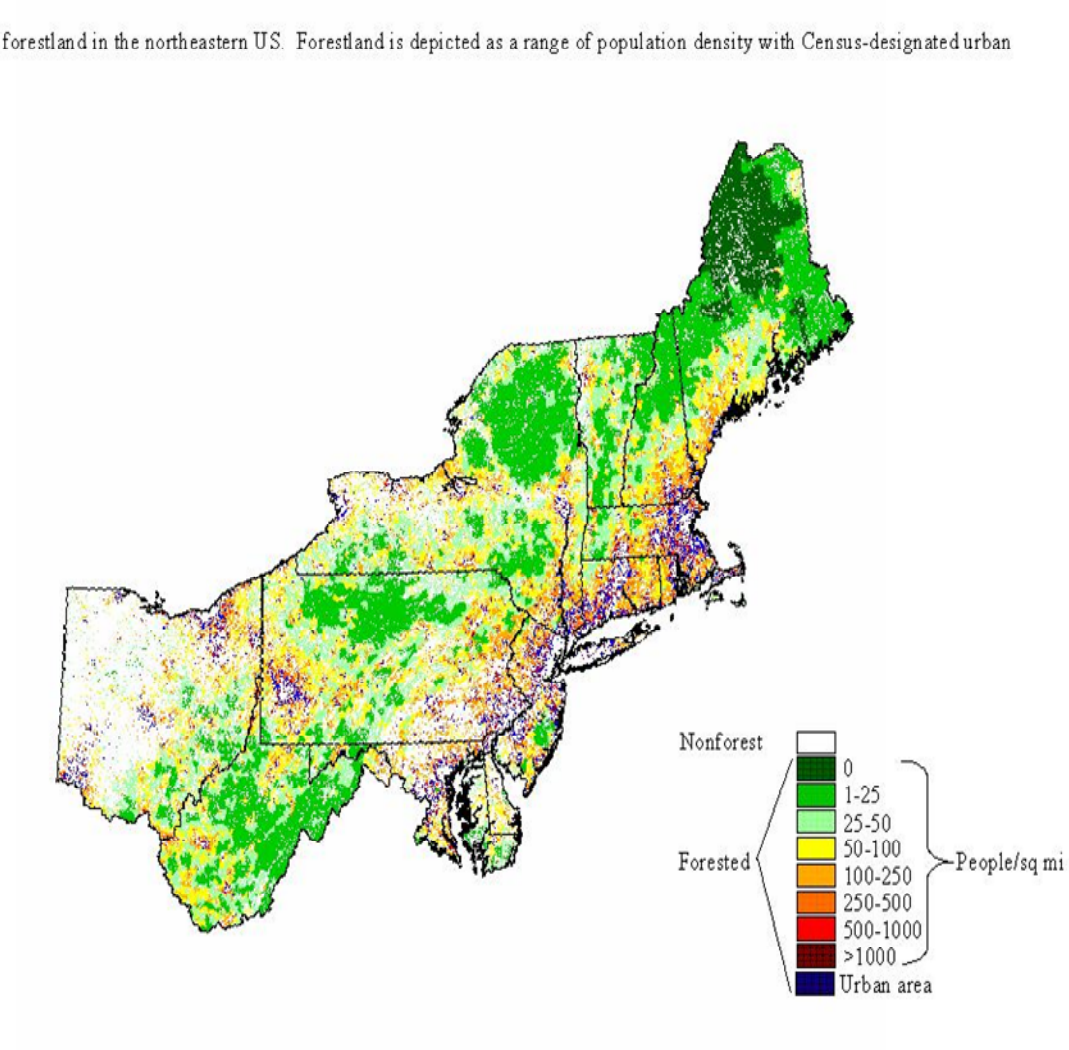

Figure 1.1. Population density and degree of forestation of the NEUS (U.S. Forest Service 2010).

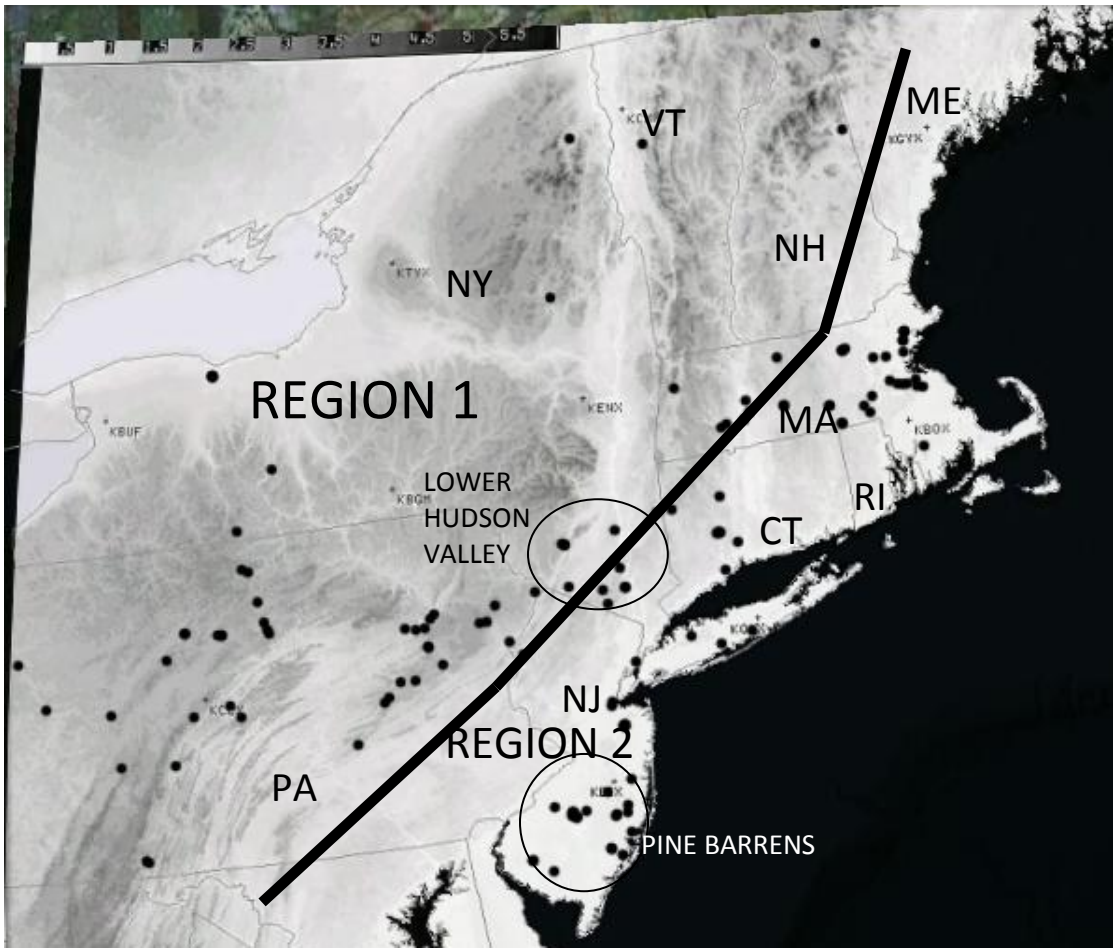

Figure 2.1. Topographical map of the NEUS and the two regions used in this study. The dots represent locations of major fires (> 100 Acres) from 1999-2009. 155 events total obtained from the Northeast Interagency Coordination Center and Pennsylvania Bureau of Forestry.

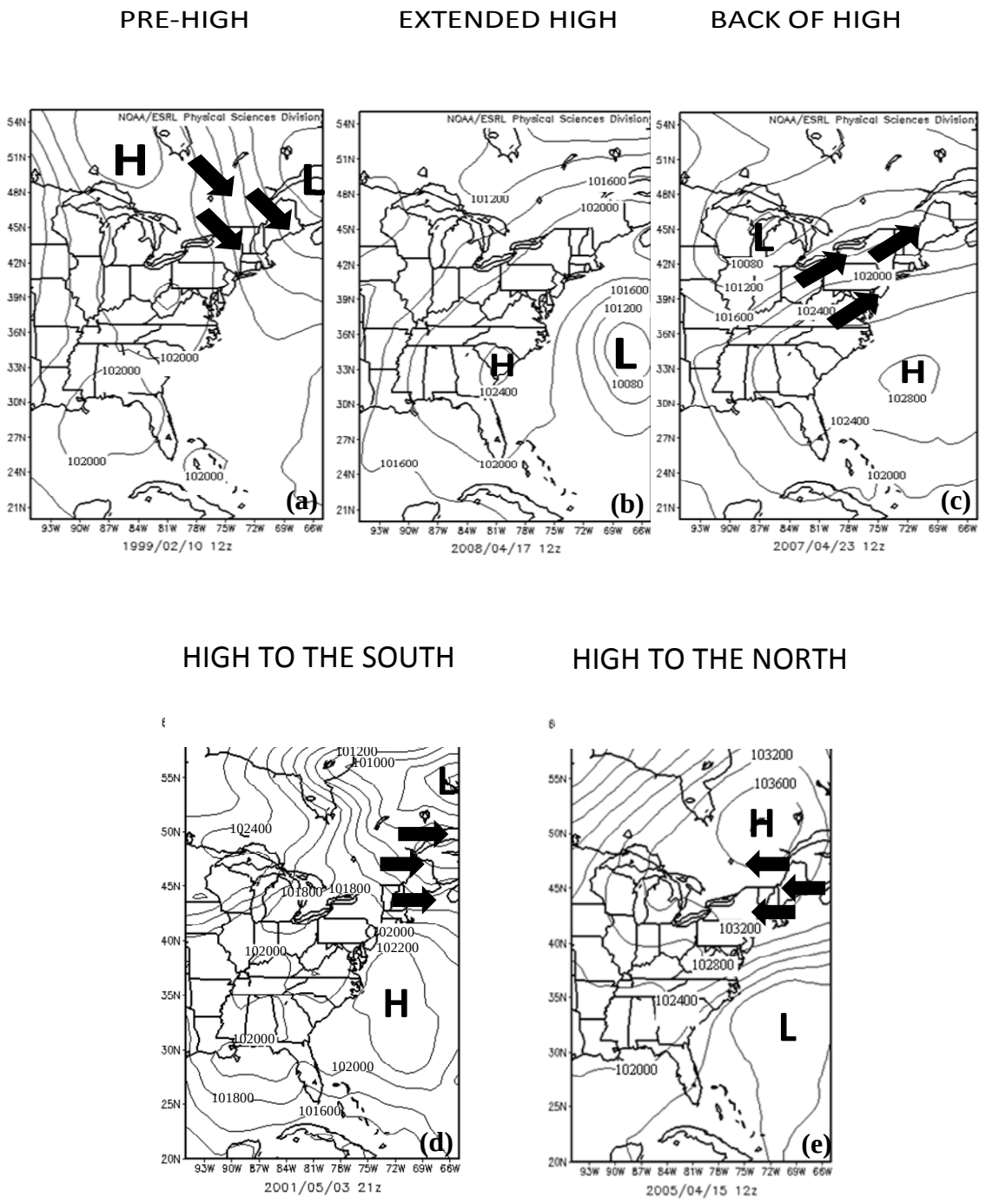

Figure 2.2. Representations of the Yarnal synoptic classification scheme showing sea-level pressure every 400 Pa (4 hPa) for (a) pre-high, (b) back of high, (c) extended high, (d) high to the south, and (e) high to the north.

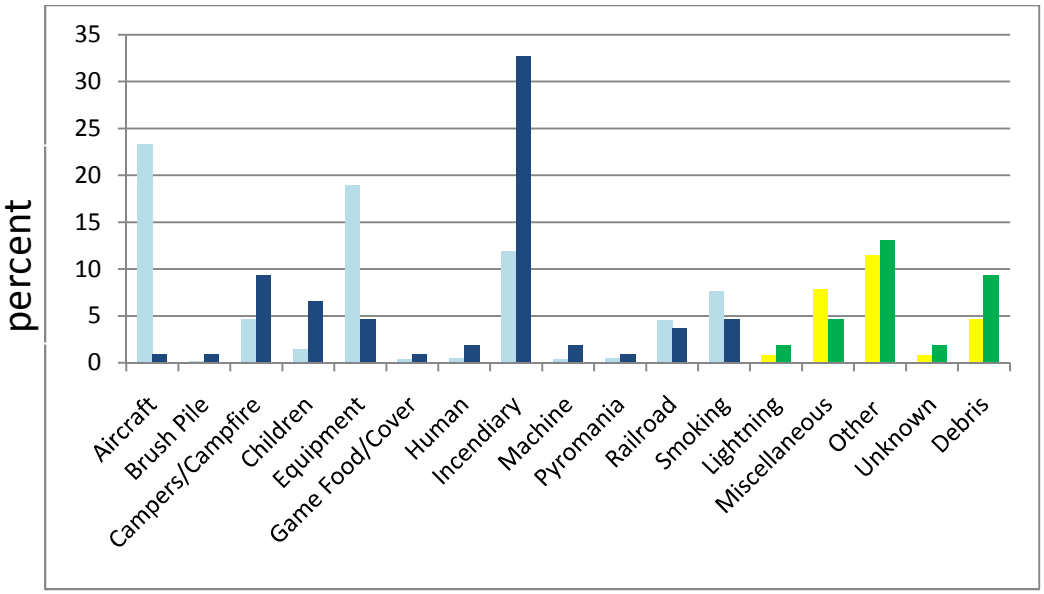

Figure 3.1. Causes of major wildfires from Jan 1999-Dec. 2009. Light blue – **acres** burned by **humans**. Dark blue – **number** of fires caused by **humans**. Yellow – **acres** burned by **other than human means**…e.g. nature. Green – **number** of fires caused by **other than human means**.

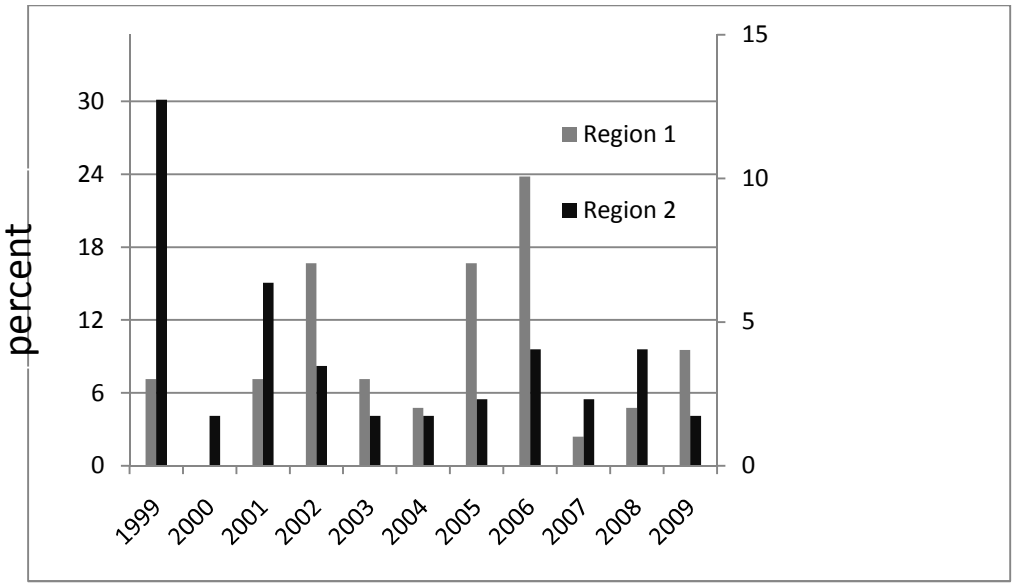

Figure 3.2. Yearly climatology for the NEUS for actual fires.

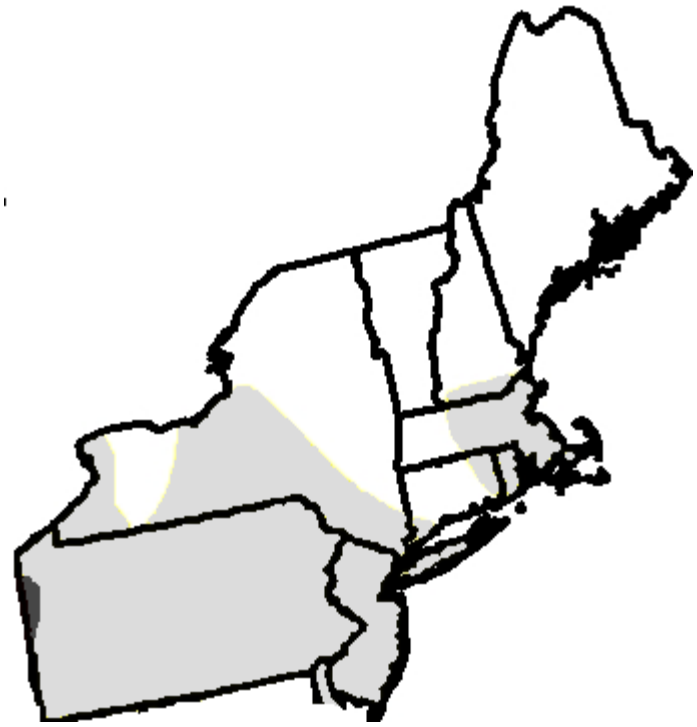

Figure 3.3. U.S. Drought Monitor for the week of 9 May 2006. Light gray denotes D0 – abnormally dry. Dark gray denotes D1 – moderate drought.

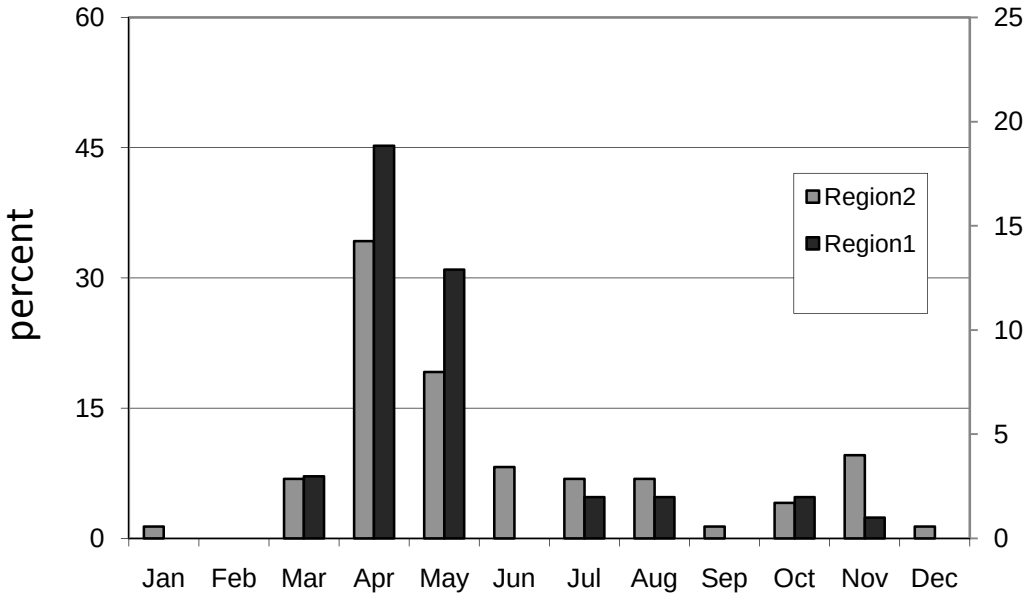

Figure 3.4. Monthly climatology for the NEUS for actual fires.

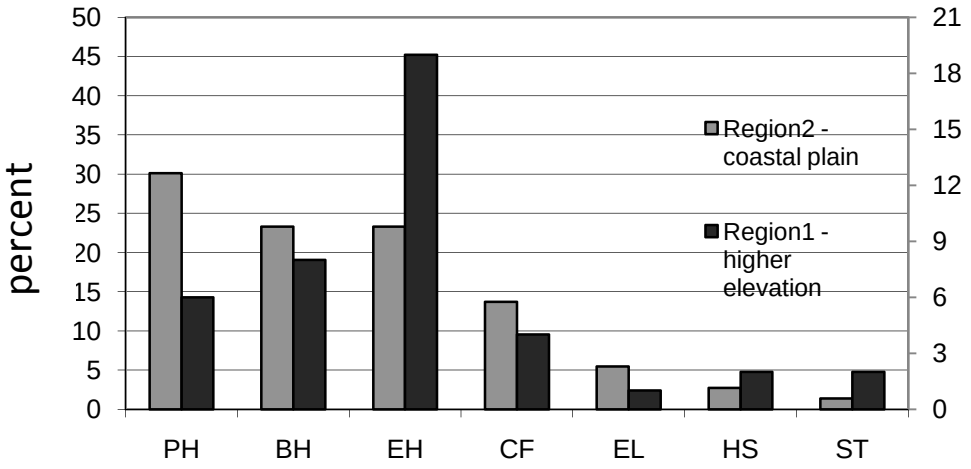

Figure 3.5. Yarnal synoptic classification climatology for the NEUS for actual fires.

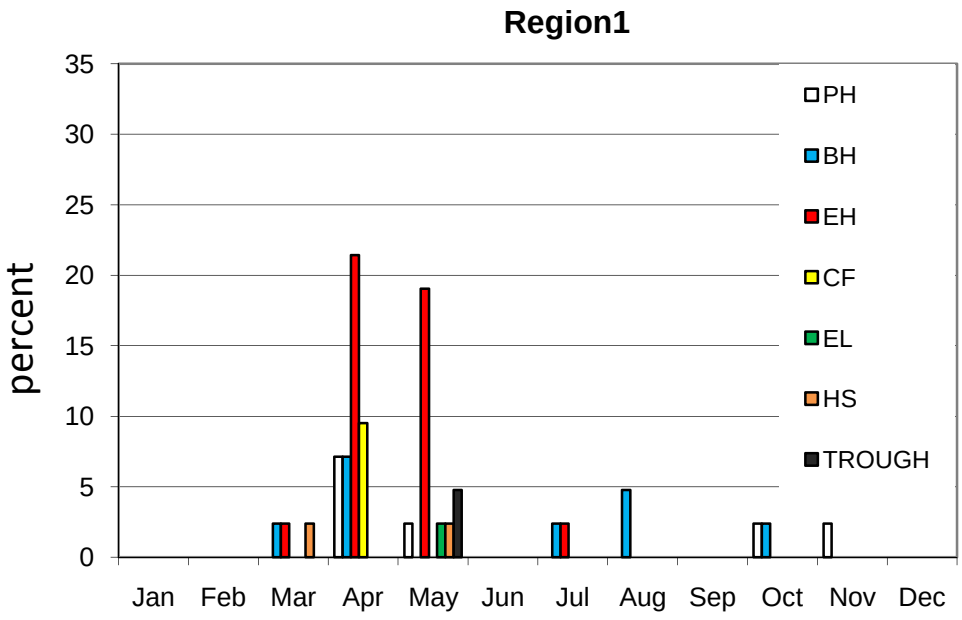

Figure 3.6. Monthly Yarnal synoptic classification climatology for the NEUS for region 1 for actual fires.

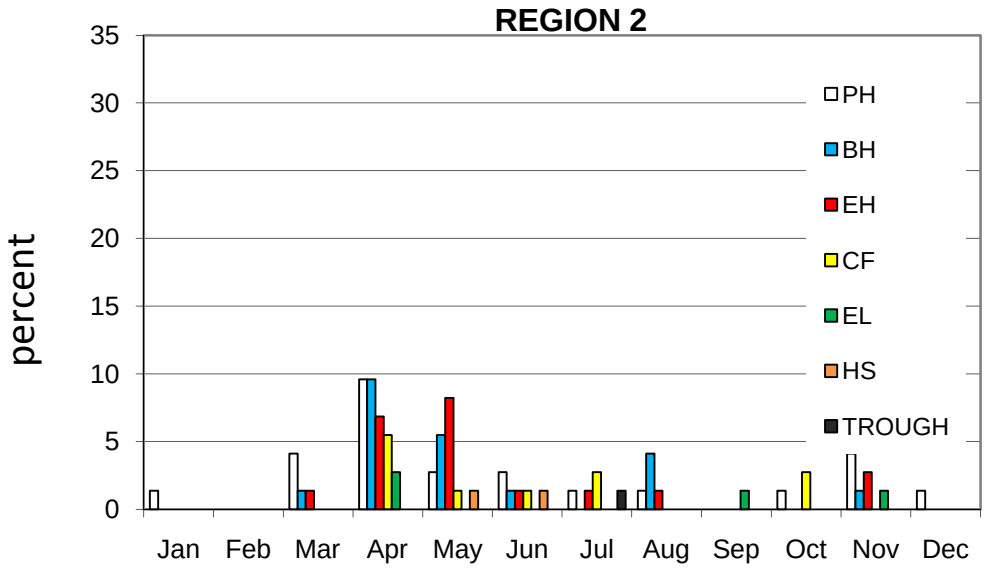

Figure 3.7. Monthly Yarnal synoptic classification climatology for the NEUS for region 2 for actual fires.

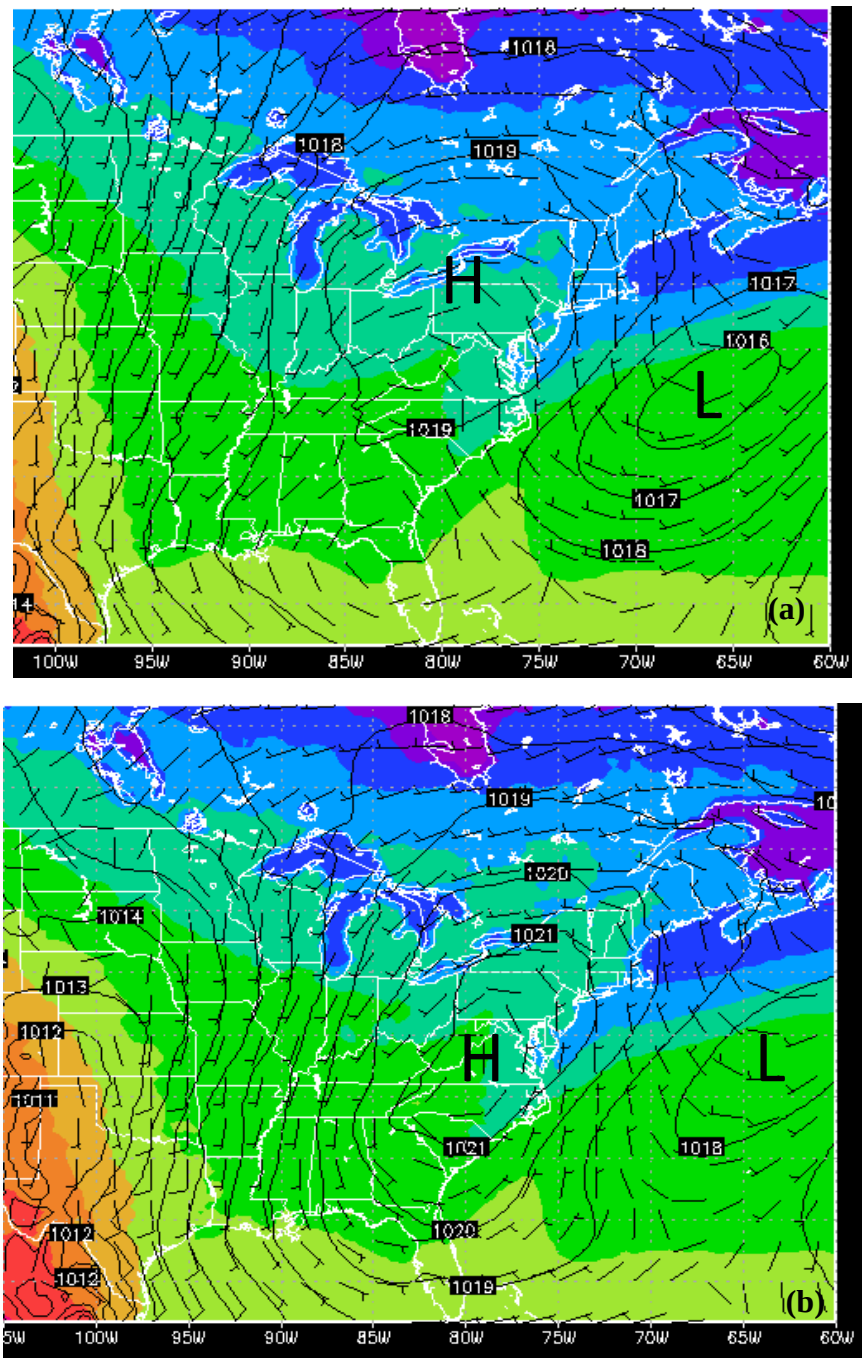

Figure 3.8. Temporal evolution of MSLP in hPa (solid line), potential temperature in Kelvin (shaded), 925 winds in m s^{-1} (half barb=5 m s^{-1}, full barb=10 m s^{-1}) for region 1 for (a) 48 hours prior to events and (b) day of events.

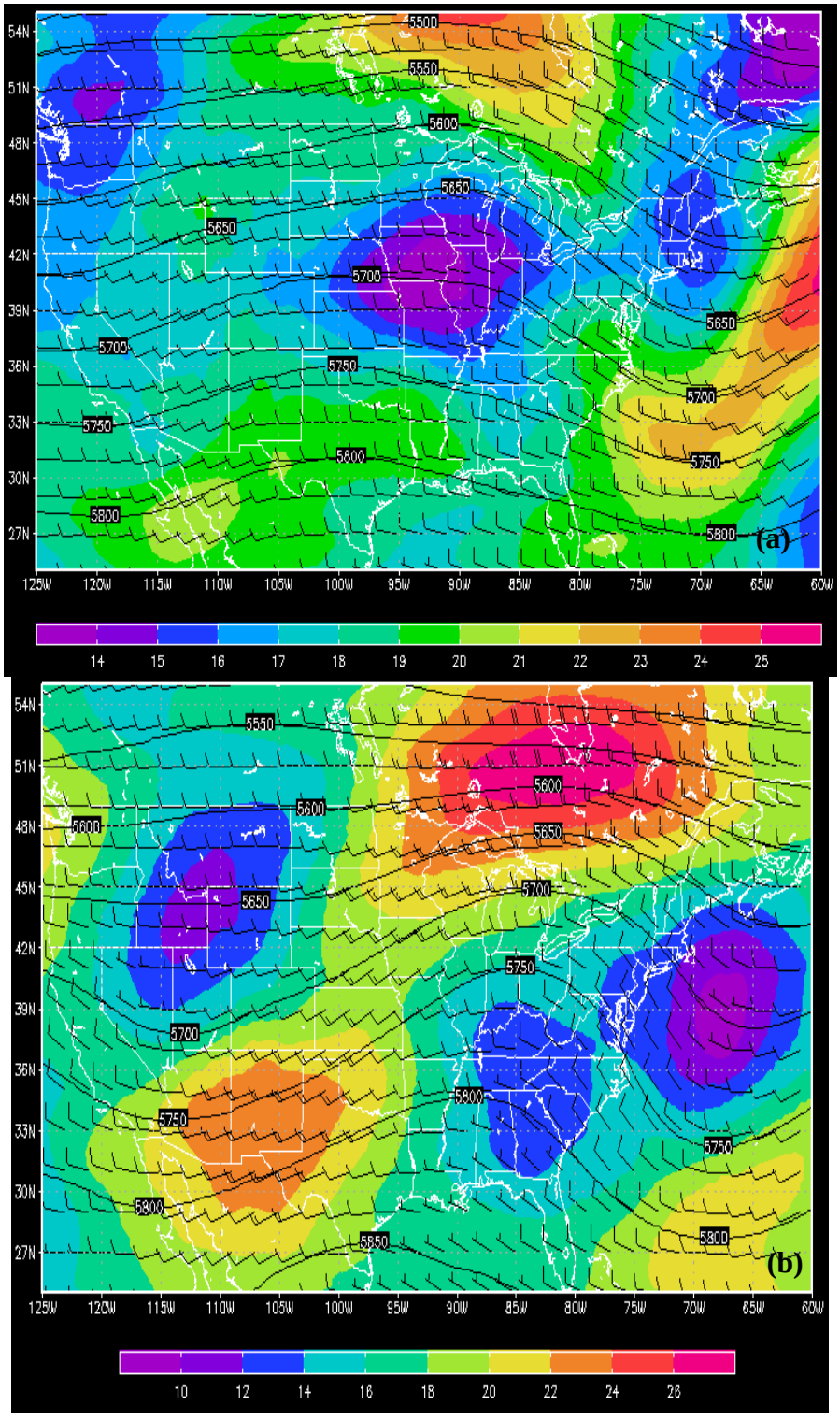

Figure 3.9. 500 hPa heights in decameters (solid line), winds in m s^{-1} (half barb=5 m s^{-1}, full barb=10 m s^{-1}), and 300 hPa wind speed in m s^{-1} (shaded) for region 1 at 2100 UTC for (a) 48 hours prior to events and (b) day of the events.

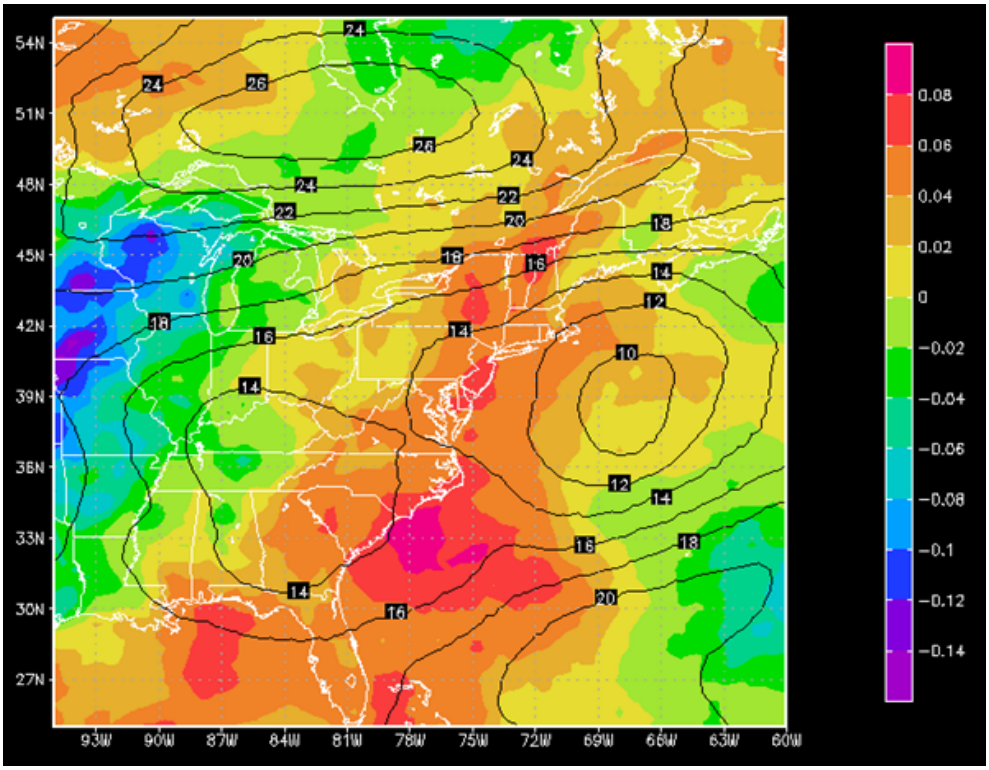

Figure 3.10. Composite of 600-300 hPa average vertical velocity in Pa/s (shaded) and 300 hPa winds (contour) for region 1 at t0.

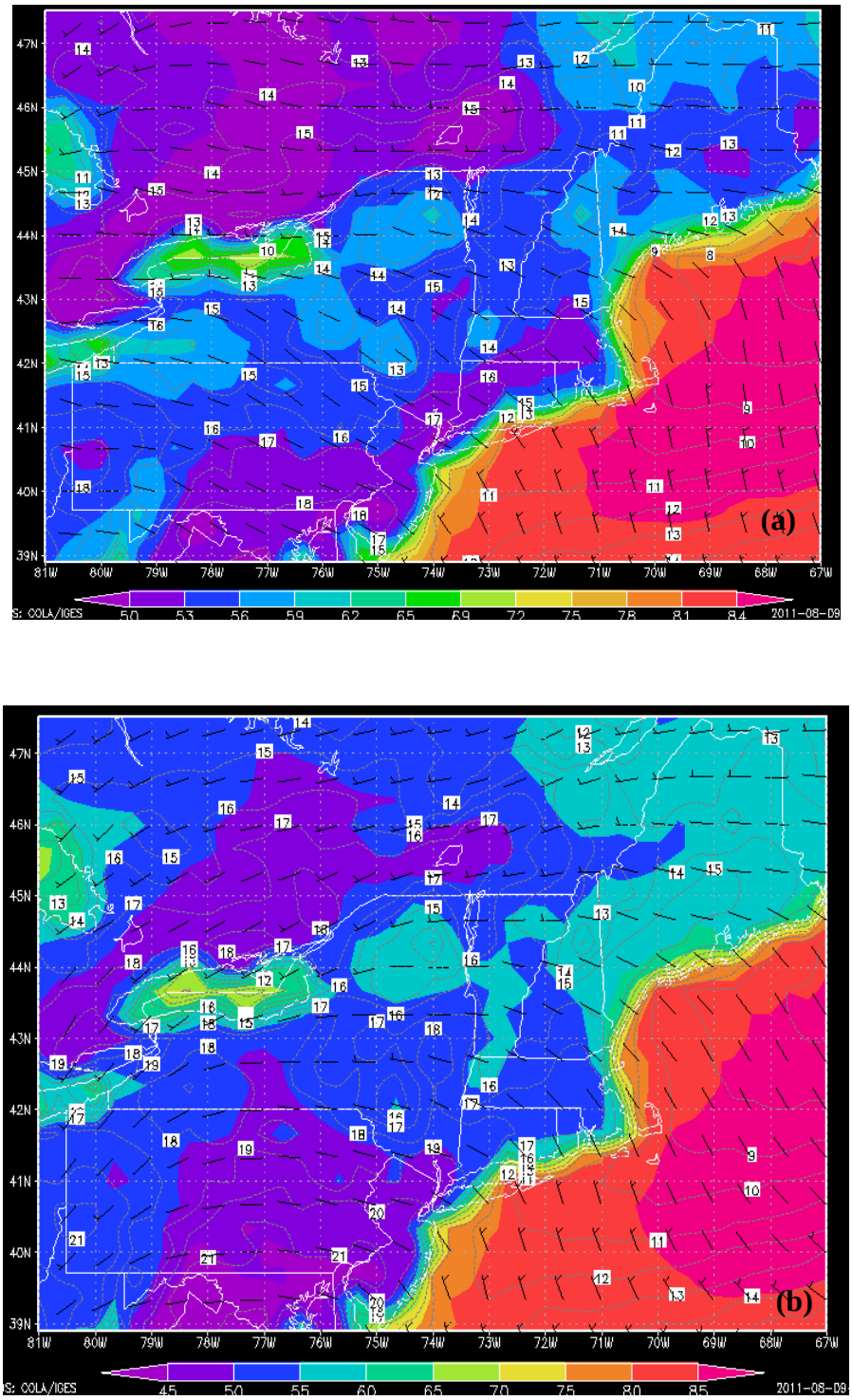

Figure 3.11. 2-m RH (shaded) and temperature in Celsius (dashed line) and 925 hPa winds in m s^{-1} (half barb=5 m s^{-1}, full barb=10 m s^{-1}) for region 1 for (a) 48 hours prior to event and (b) day of the event.

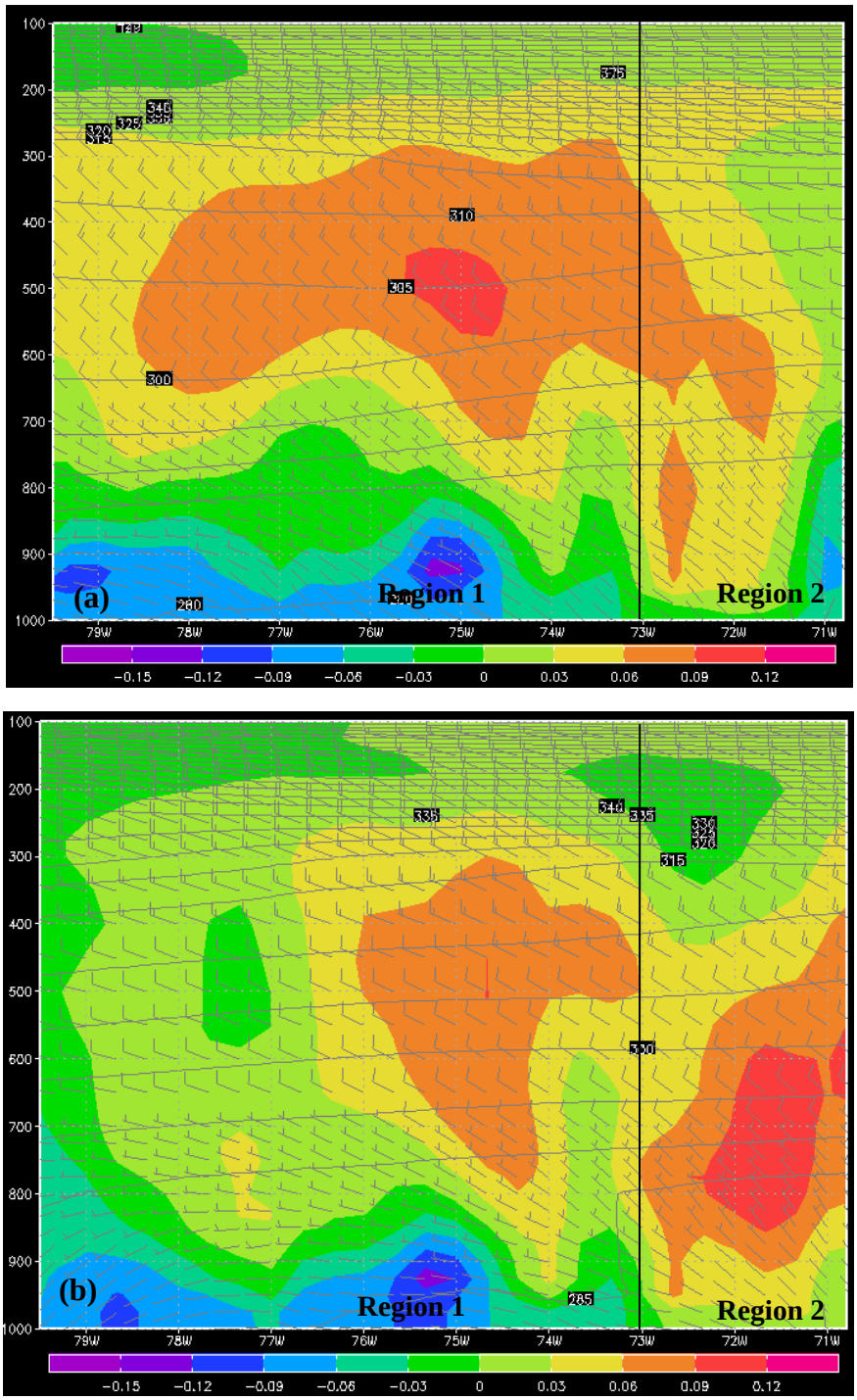

Figure 3.12. Cross section along 42.0N with potential temperature in Kelvin (contours), vertical velocity in Pa/s (shaded), and winds in m s^{-1} (half barb=5 m s^{-1}, full barb=10 m s^{-1}) for region 1 at (a) 48 hours prior to events and (b) day of the events. The vertical line divides region 1 and region 2.

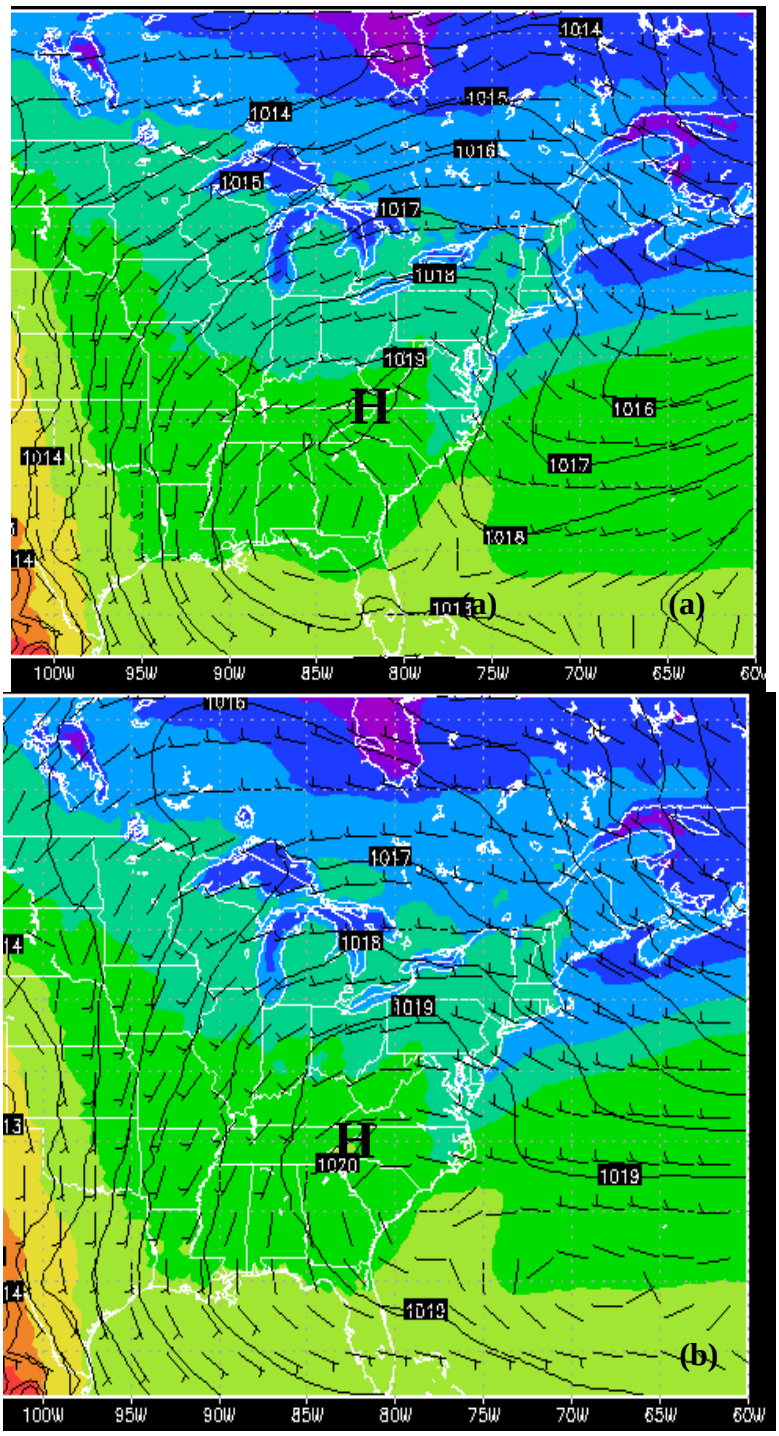

Figure 3.13. Same as in figure 3.8 but for region 2.

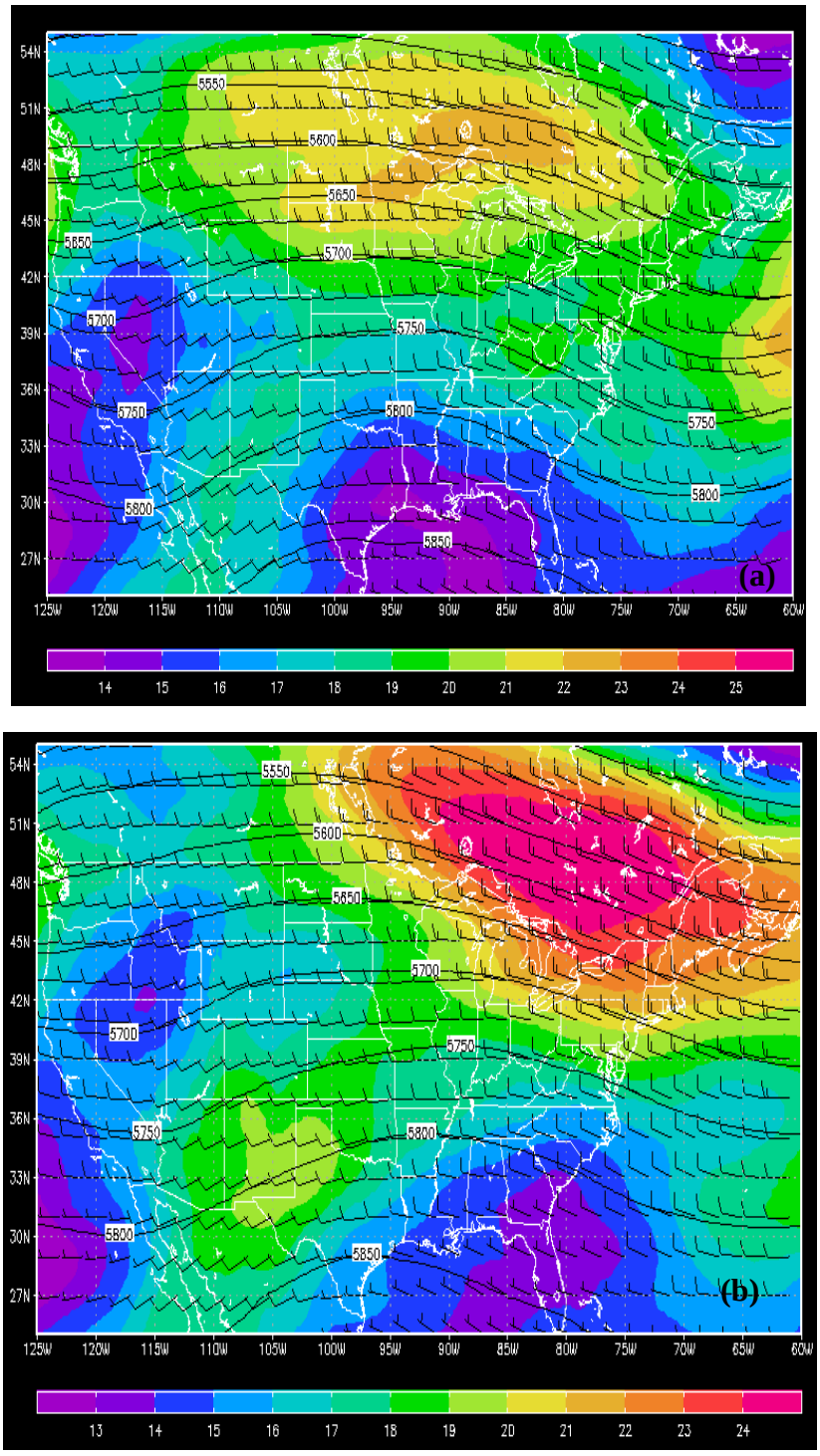

Figure 3.14. Same as in figure 3.9 but for region 2.

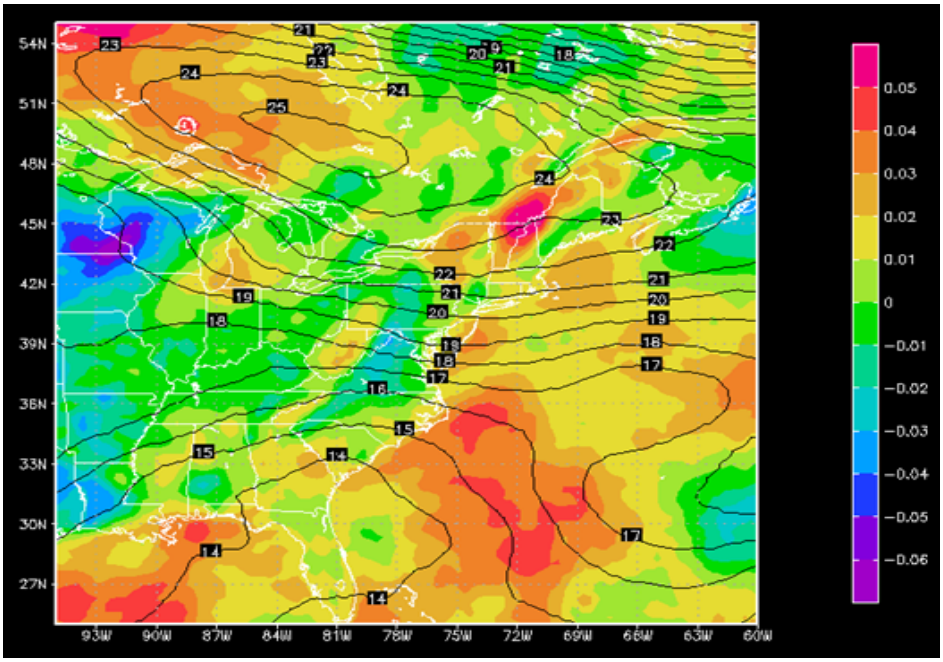

Figure 3.15. Same as in figure 3.10, but for region 2.

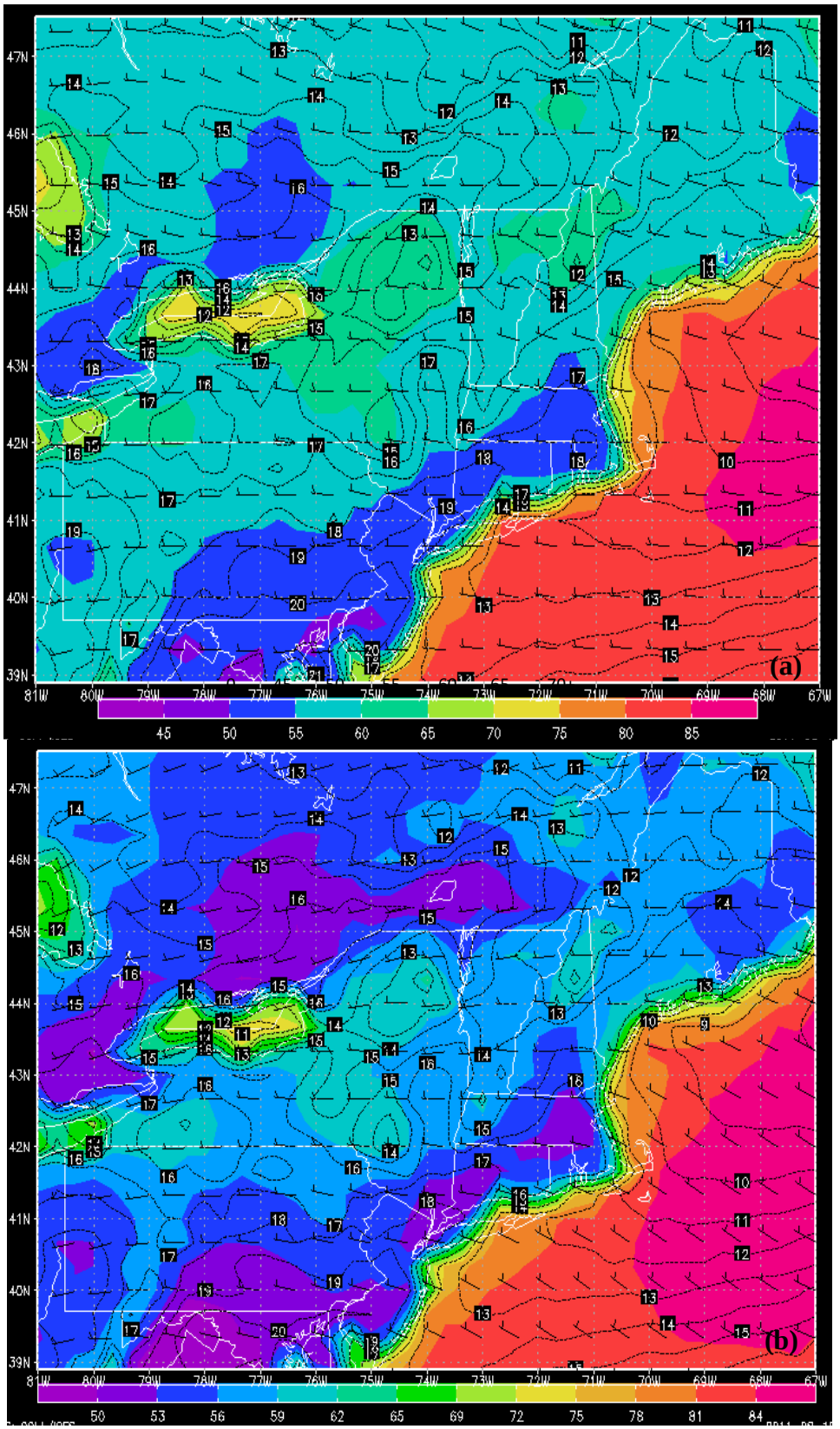

Figure 3.16. Same as in figure 3.11, but for region 2.

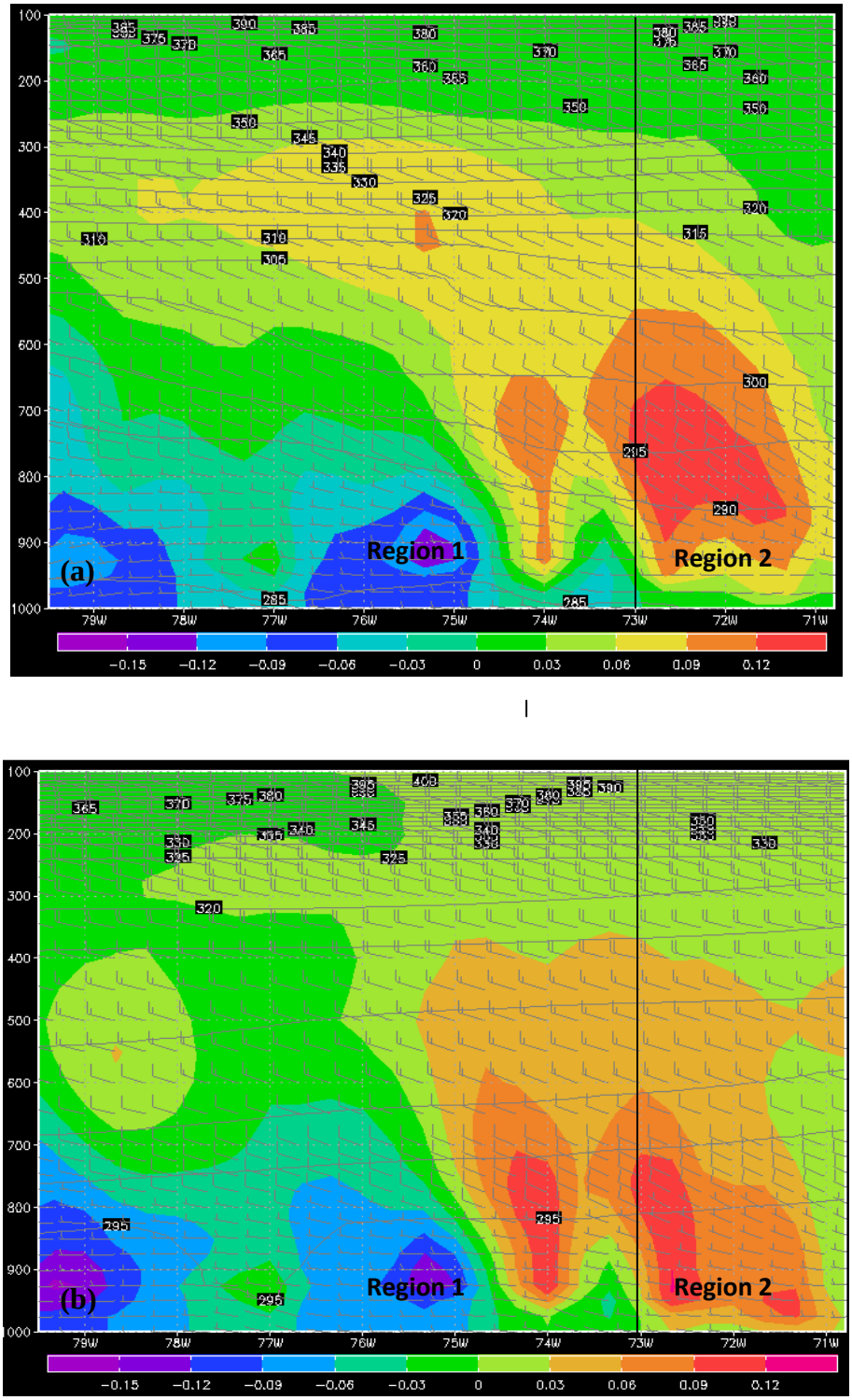

Figure 3.17. Same as in figure 3.12, but for region 2.

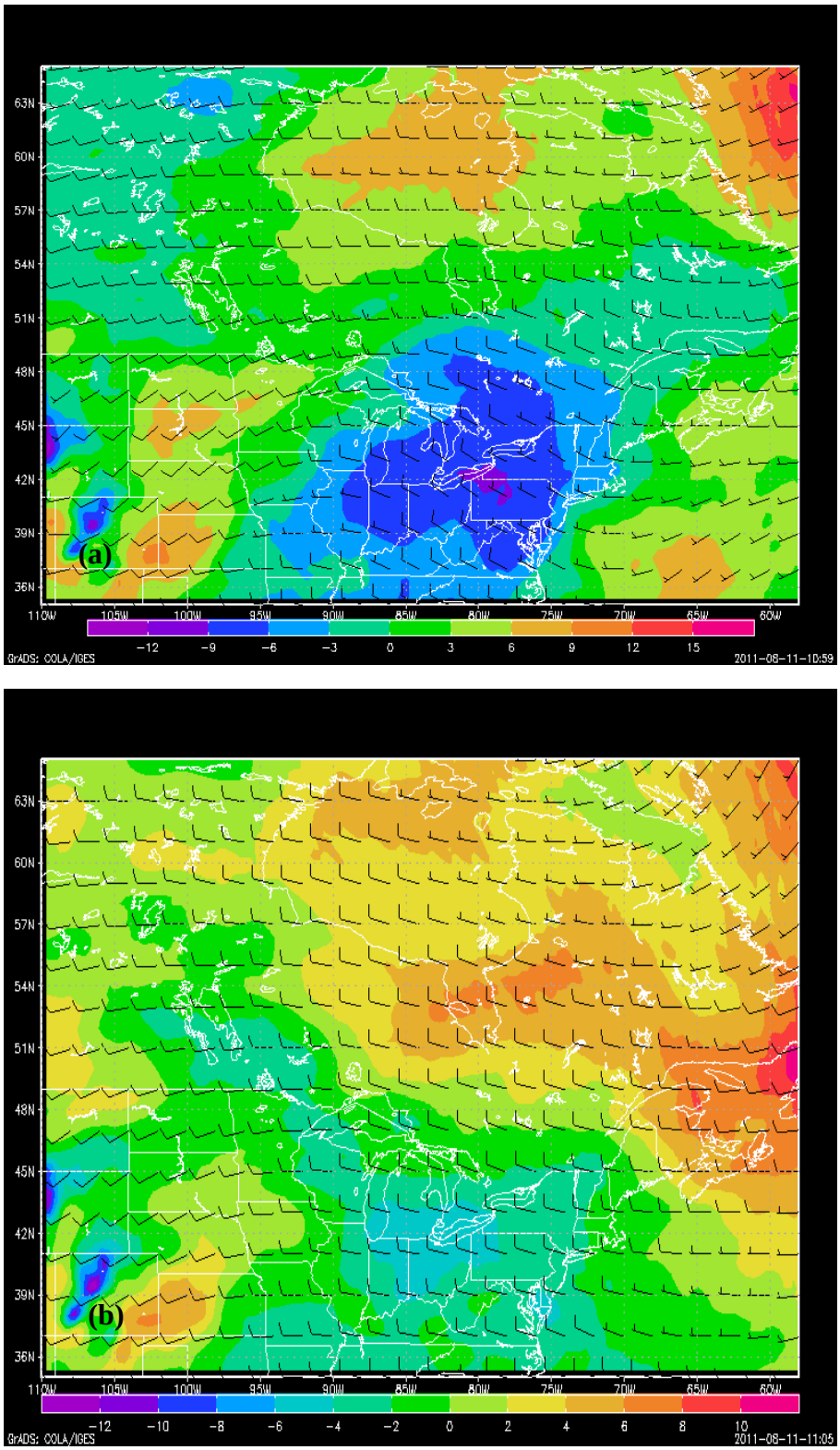

Figure 3.18. Composite of 600-300 hPa thermal wind (half barb=5 m s^{-1}, full barb=10 m s^{-1}) and term A (shaded) from the Sutcliffe-Trenberth form of the QG omega equation or region for a) region 1 and b) region2 for t0.

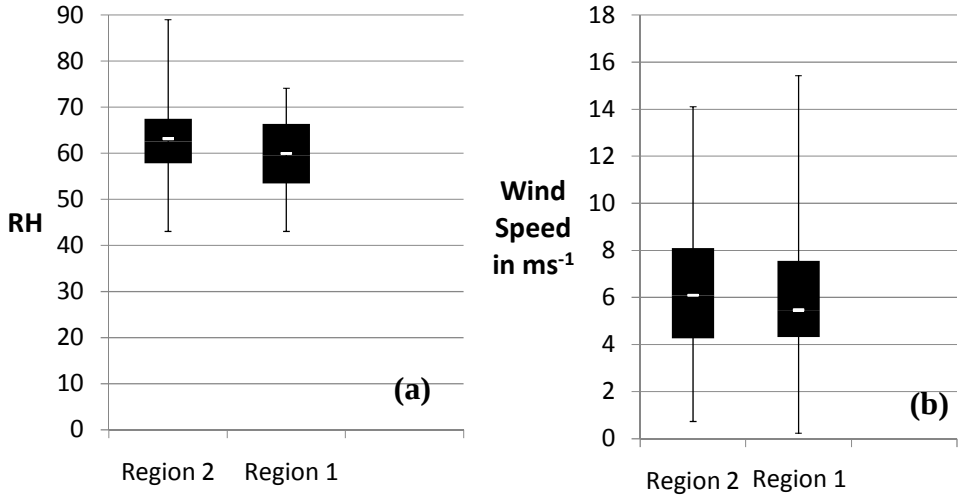

Figure 3.19. Box and whisker plot of a) RH and b) wind speed. The white line is the areal average. The lower and upper portions of the boxes represent the 25th and 75th percentile respectively, and the lower and upper whiskers represent the minimum and maximum values observed for t=0.

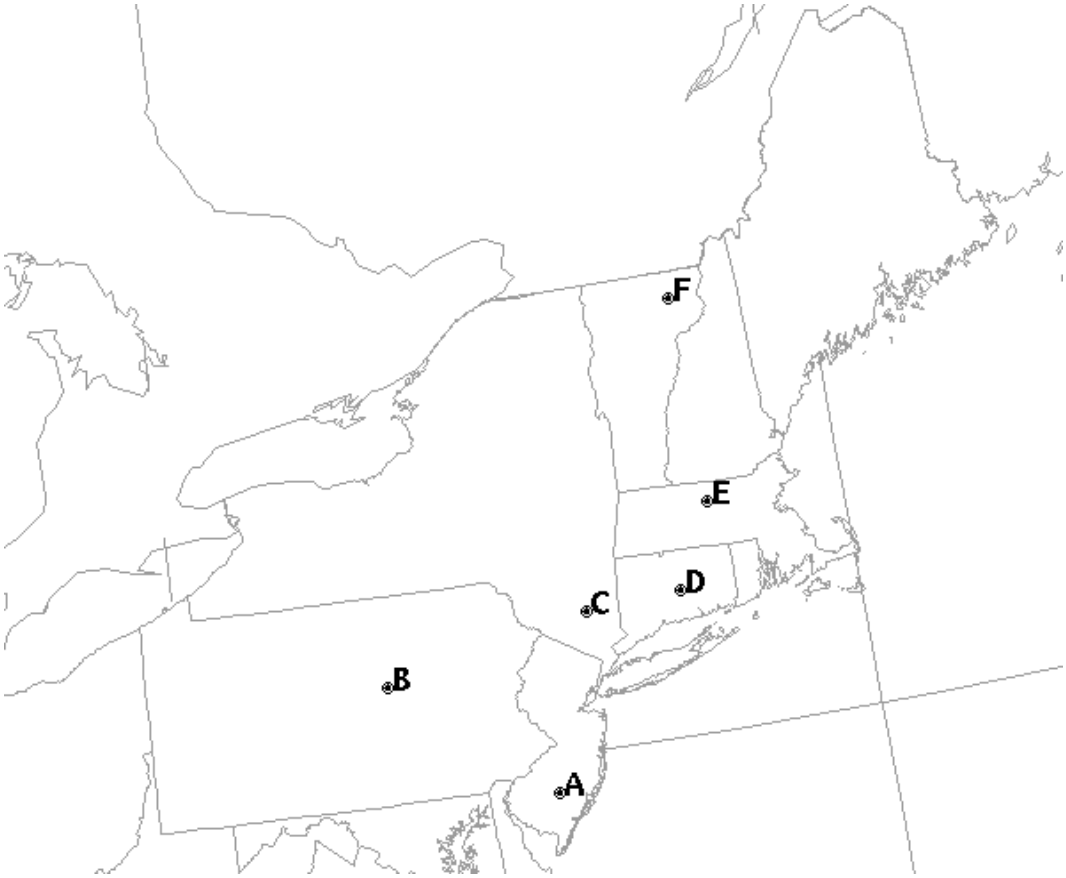

Figure 3.20. Starting points of the back trajectories A=#1, B=#2, C=#3, D=#4, E=#5, F=#6.

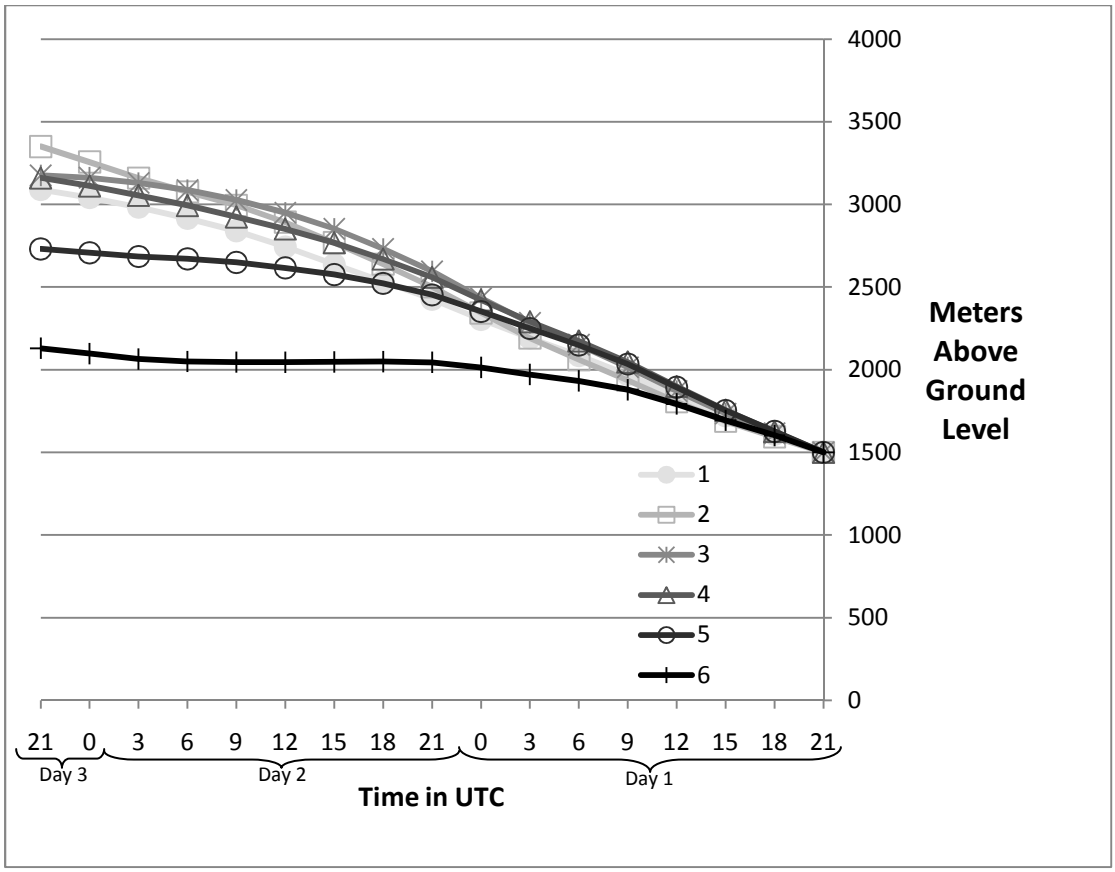

Figure 3.21. Average height of trajectories for pre-high synoptic type.

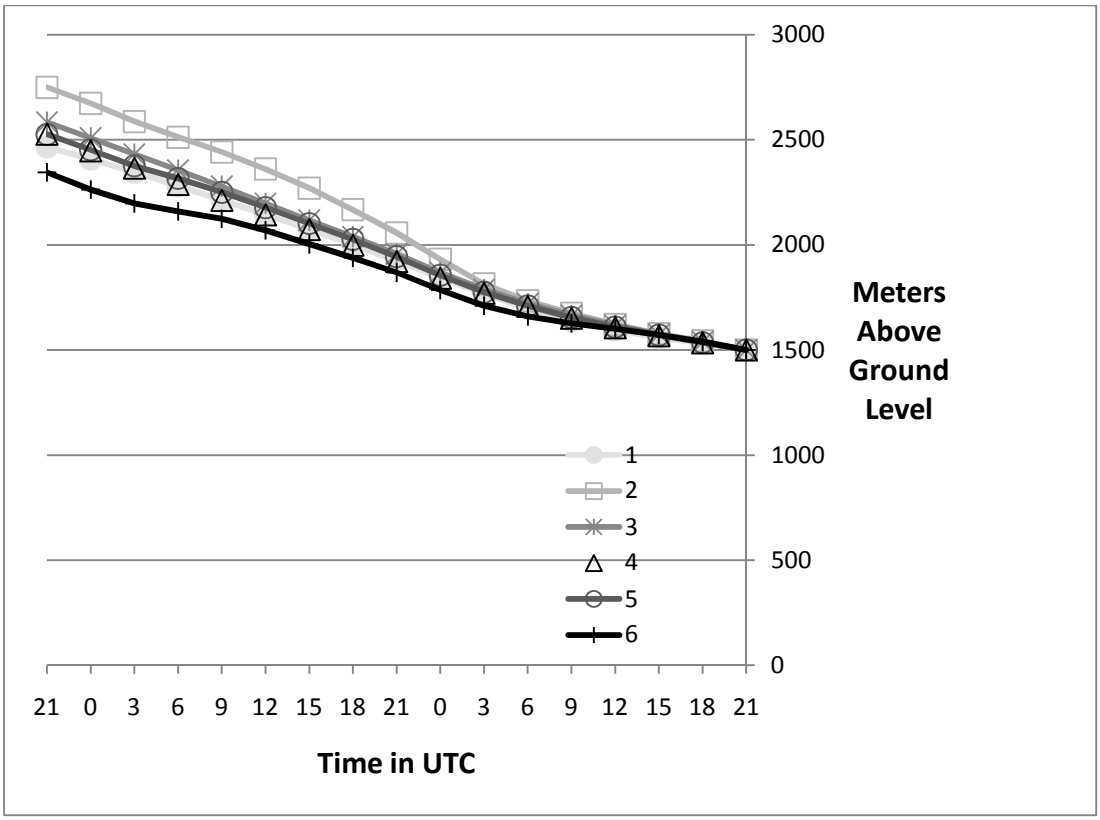

Figure 3.21. Same as in 3.18, but for the extended high synoptic type.

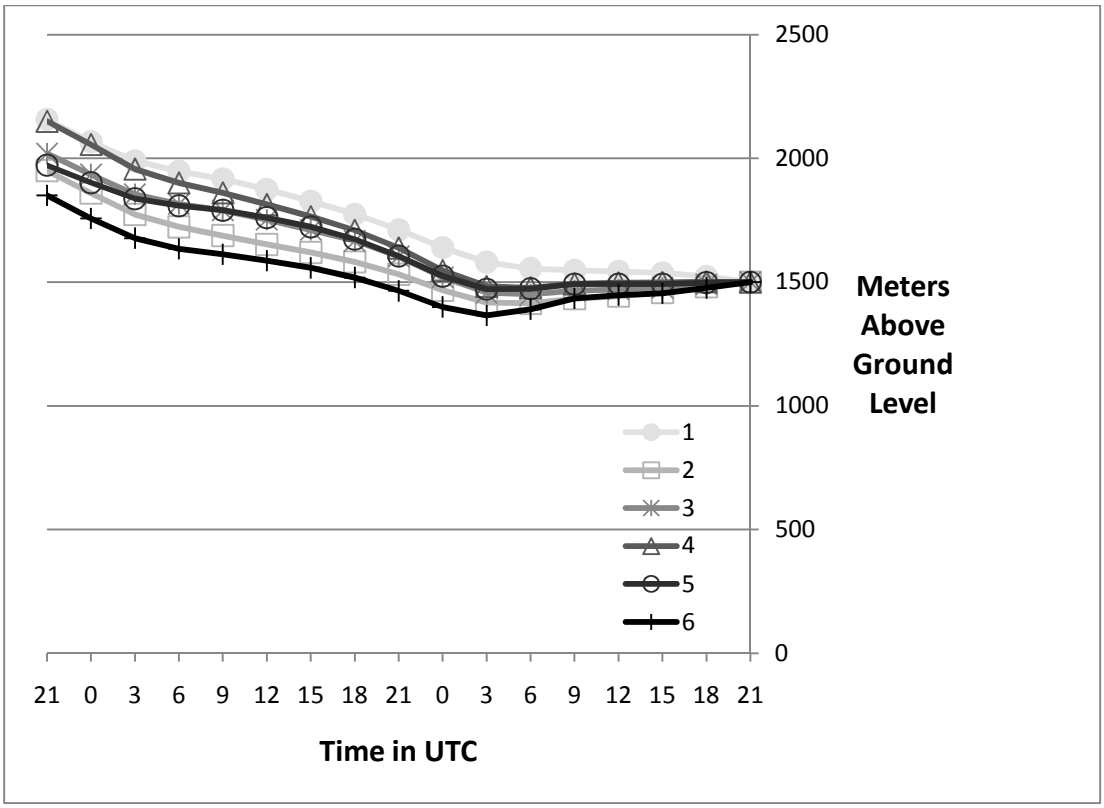

Figure 3.23. Same as in 3.21, but for back-of-high synoptic type.

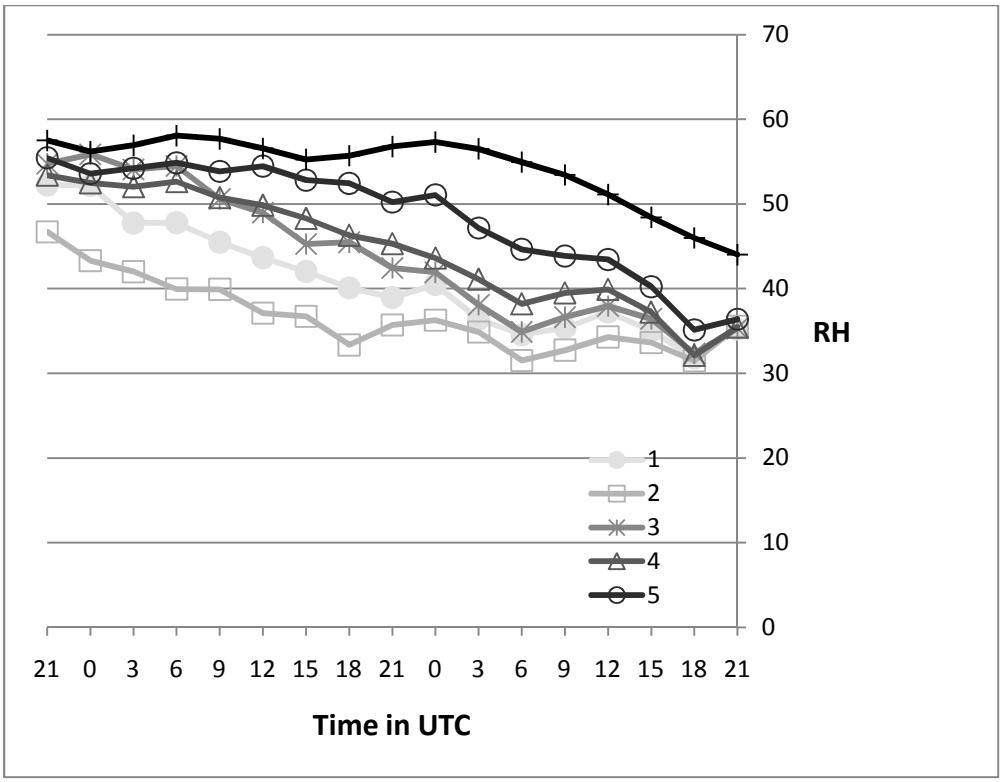

Figure 3.24. Average RH for trajectories for the pre-high synoptic type.

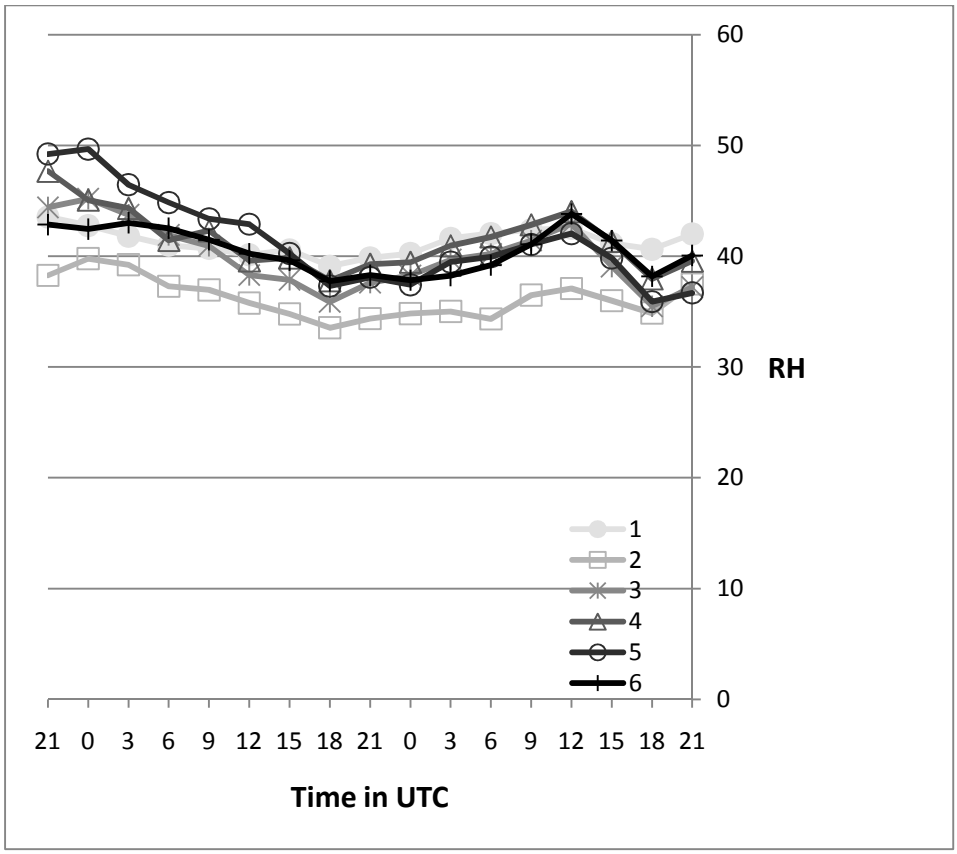

Figure 3.25. Same as in 3.24, but for the extended high synoptic type.

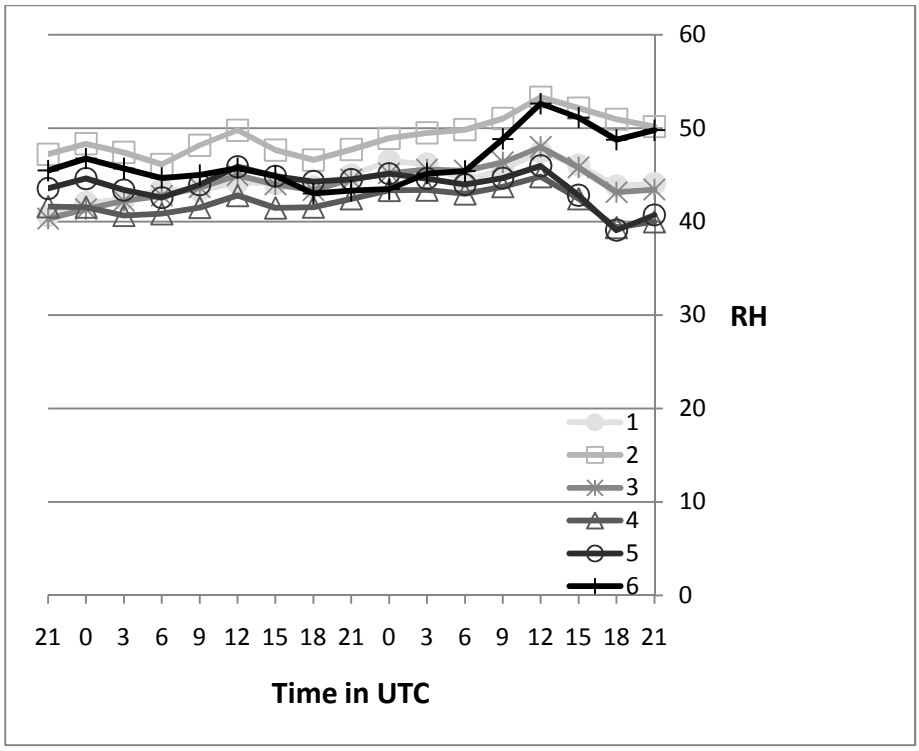

Figure 3.26. Same as in 3.24, but for back-of-high synoptic type.

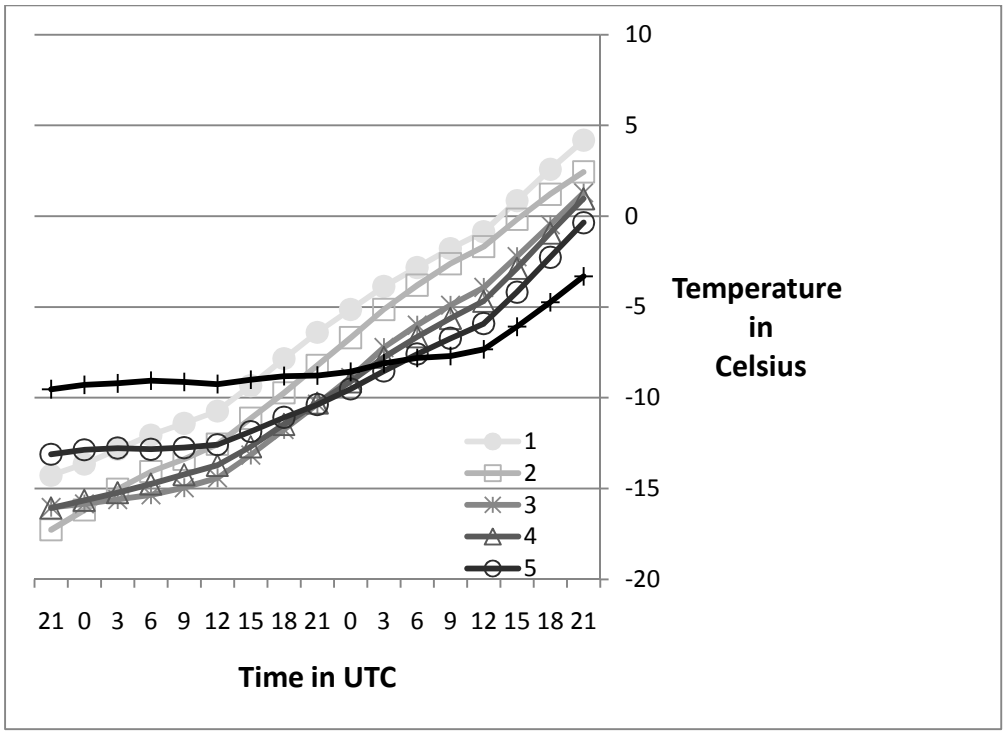

Figure 3.27. Average temperature along trajectories of pre-high synoptic type.

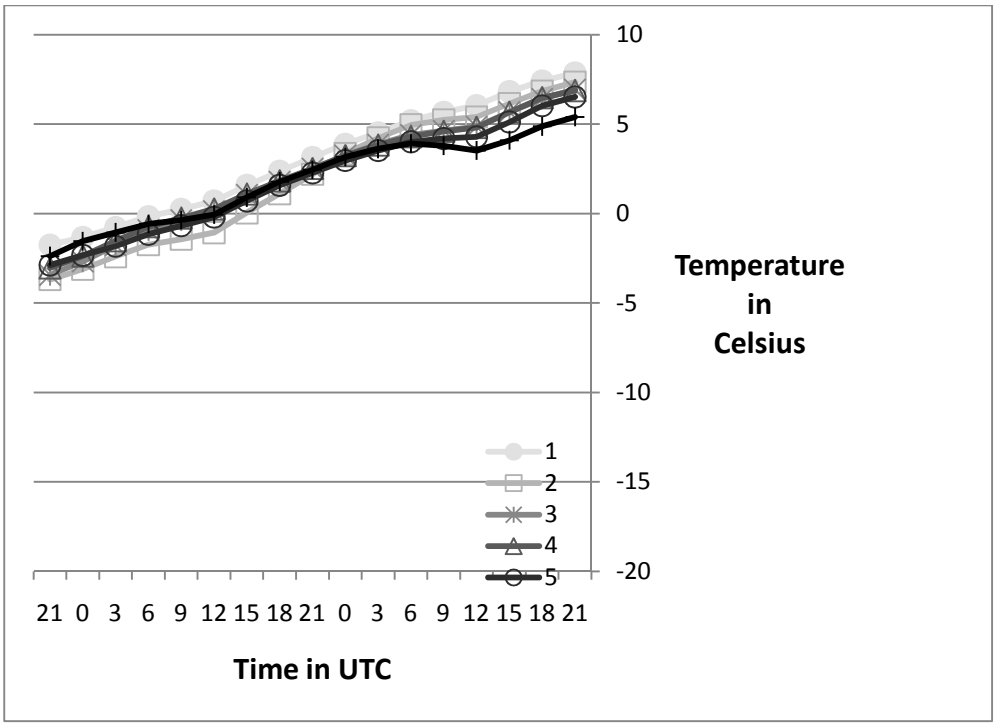

Figure 3.28. Same as in 3.27, but for extended high synoptic type.

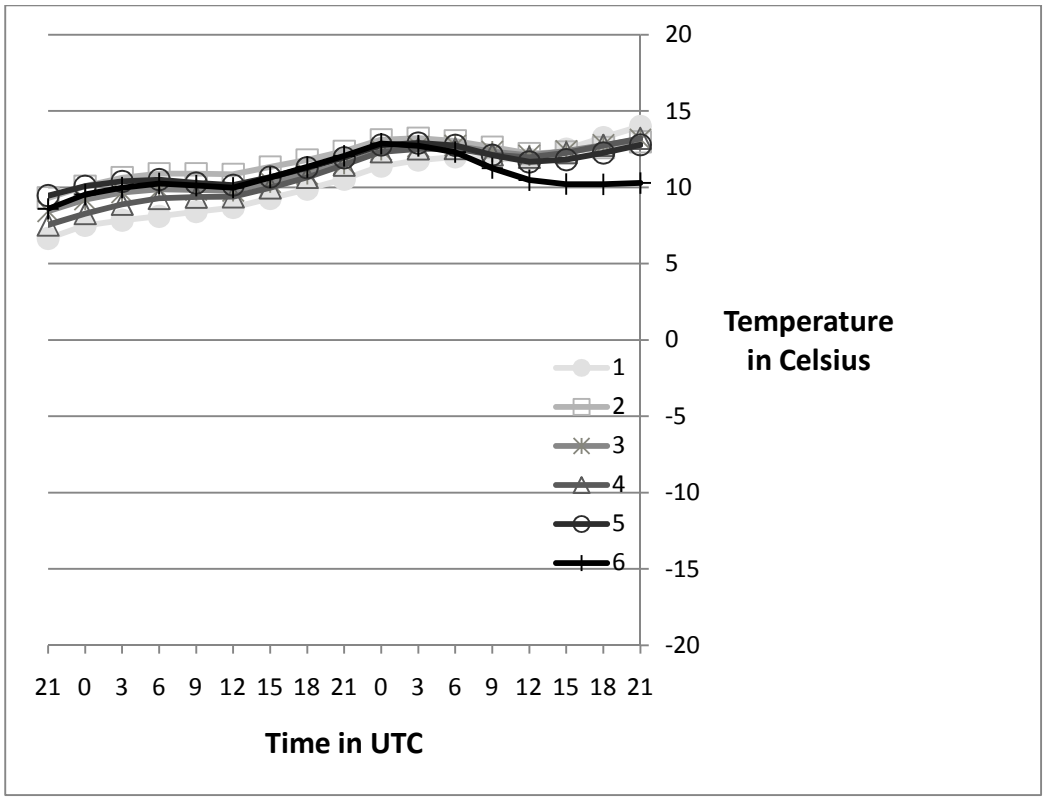

Figure 3.29. Same as in 3.27, but for back-of-high synoptic type.

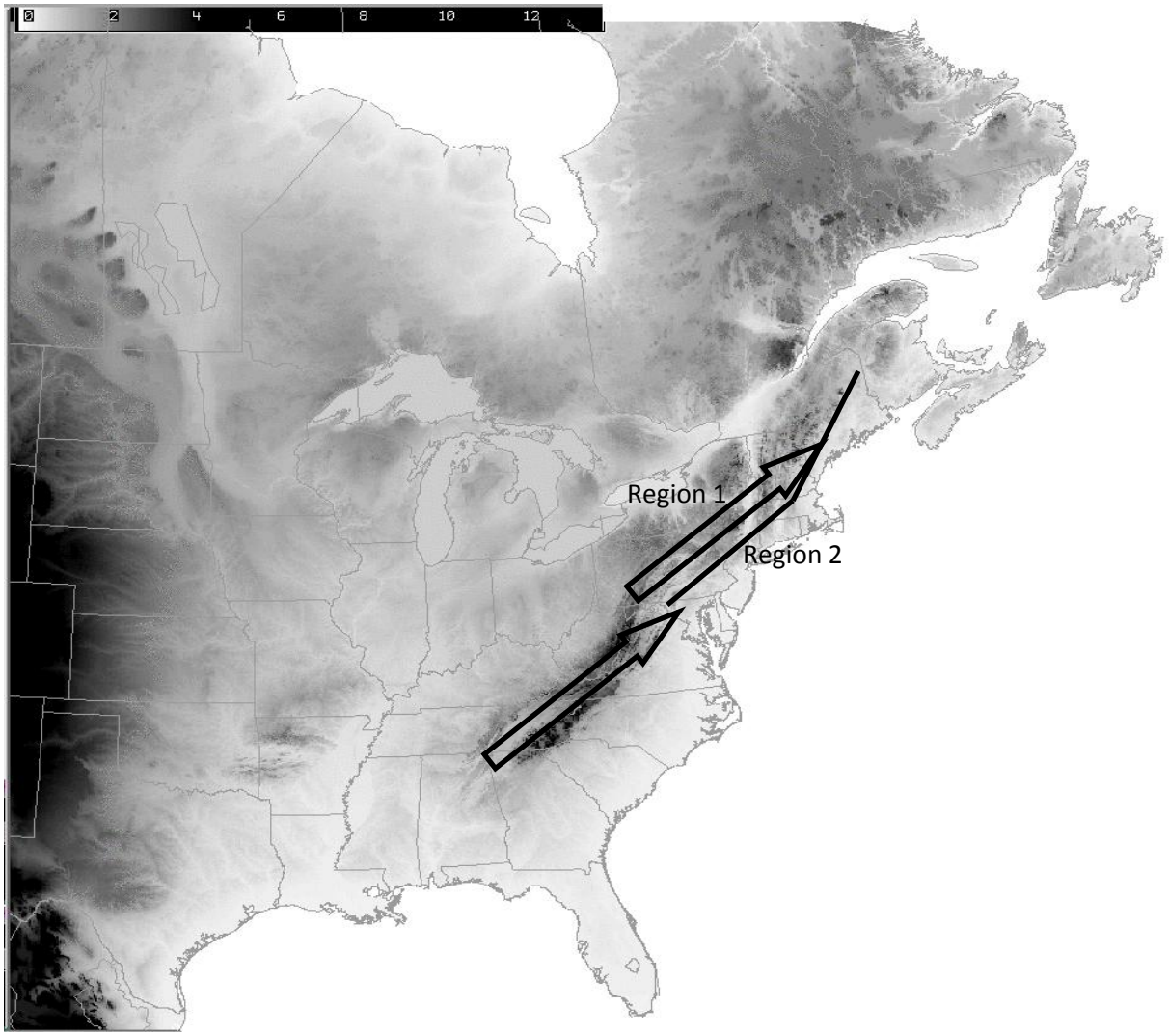

Figure 3.30. Topographical map of the NEUS. Darker colors are higher terrain, with anything above 914 meters (3000 feet) in black. The line divides region 1 and region 2. The arrows depict southwesterly flow over the Eastern U.S.

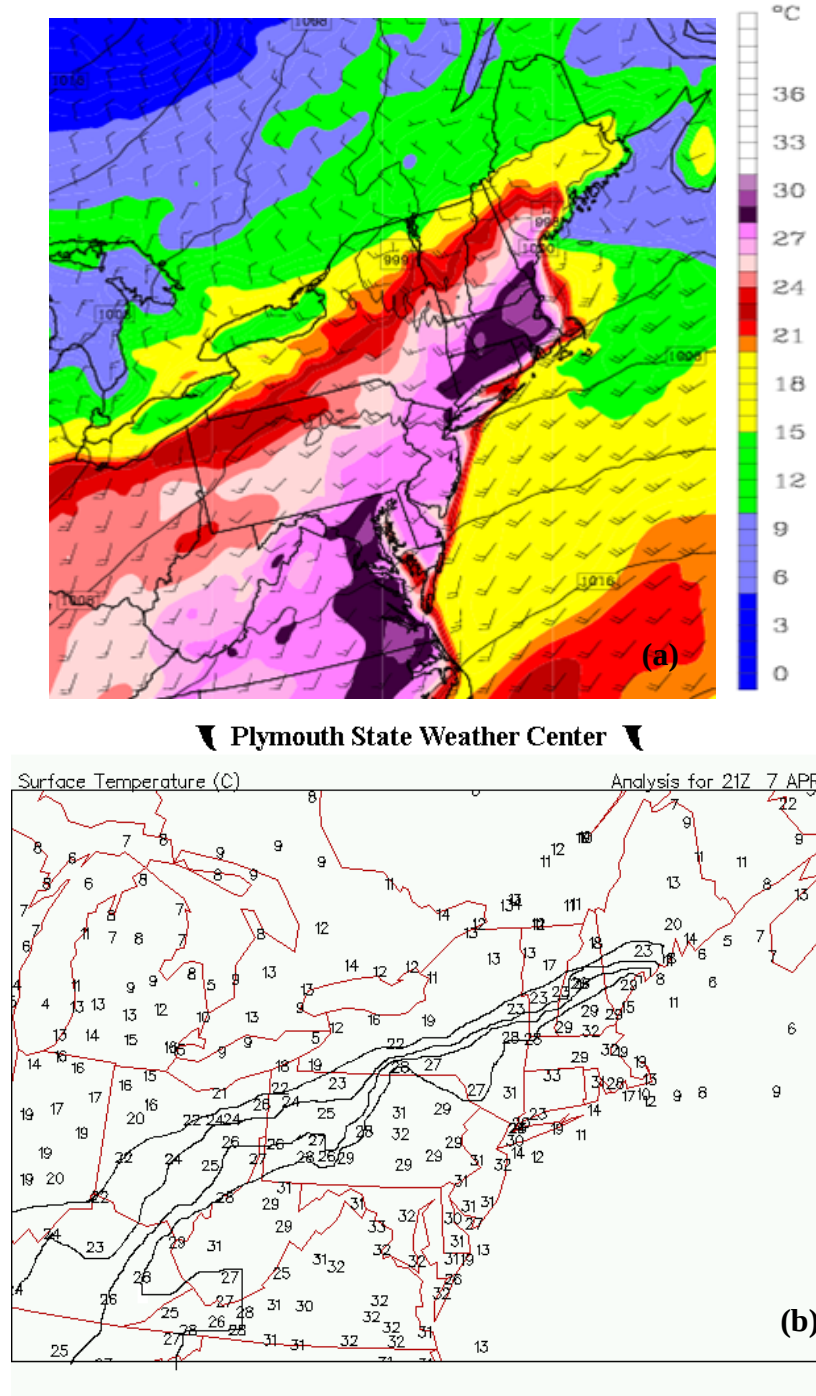

Figure 3.31. (a) Results of the control run for 7-8 April 2010 event. The forecast hour is 2100 UTC on April 7 2010. MSLP in hPa (solid lines, contoured every 4 hPa), 2-meter temperature in °C (shaded), and 10-meter wind (barbs, half wind barb is 2.5 m s^{-1}, full wind barb is 5 m s^{-1}). (b) Observations of 2-meter temperature from Plymouth State University at 2100 UTC on 8 April 2010. Contours are every 2°C from 22°C to 28°C.

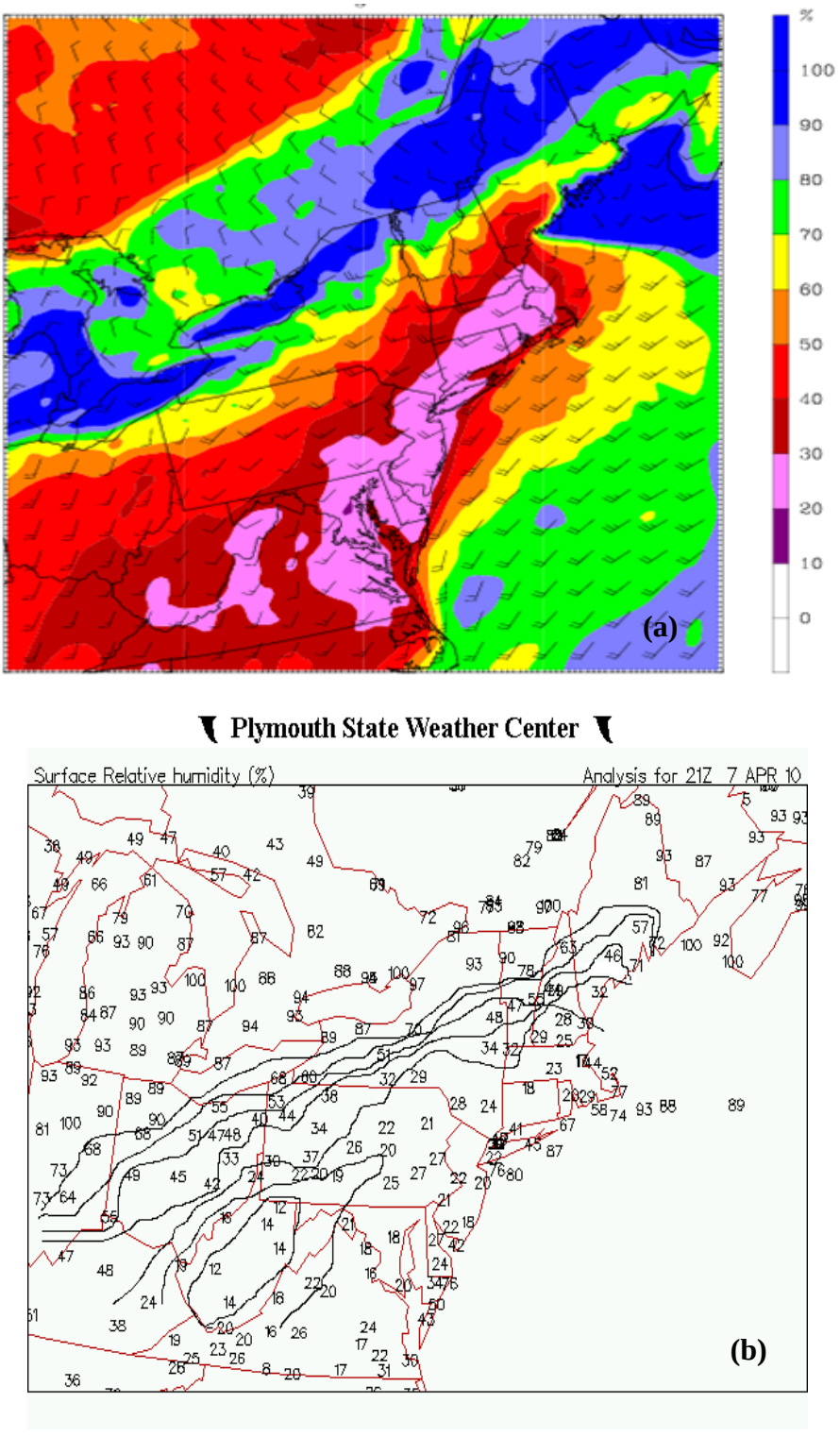

Figure 3.32. (a) Results of the control run for the 7-8 April 2010 event. The forecast hour is 2100 UTC on 7 April 2010. 2-meter temperature RH (shaded), and 10-meter winds (barb, half wind barb is 2.5 m s^{-1}, full wind barb is 5 m s^{-1}). (b) Observations of 2-meter RH from Plymouth State University for 2100 UTC on 8 April 2010. Contours are every 10% from 10%-70%.

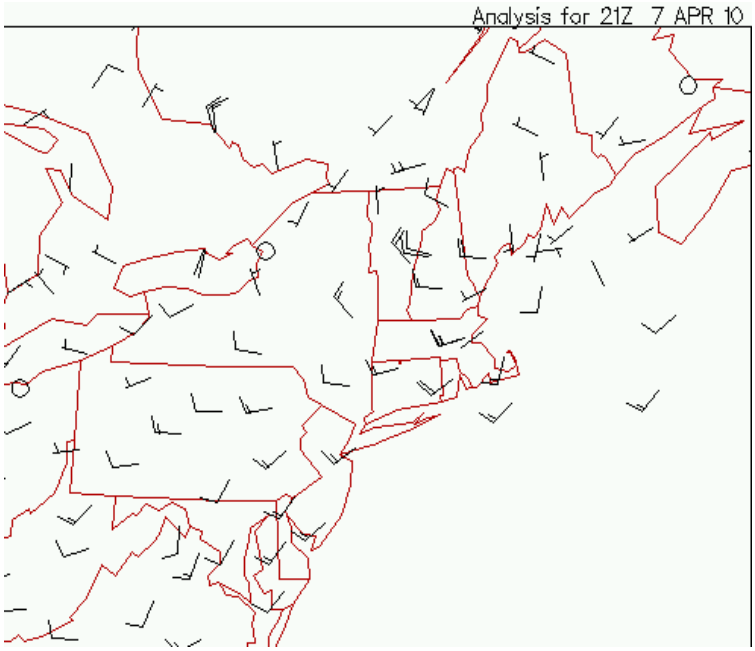

Figure 3.33. Wind observations for 7 April 2010 at 2100 UTC. Half wind barb is 2.5 m s^{-1}, full wind barb is 5 m s^{-1}. From Plymouth State University.

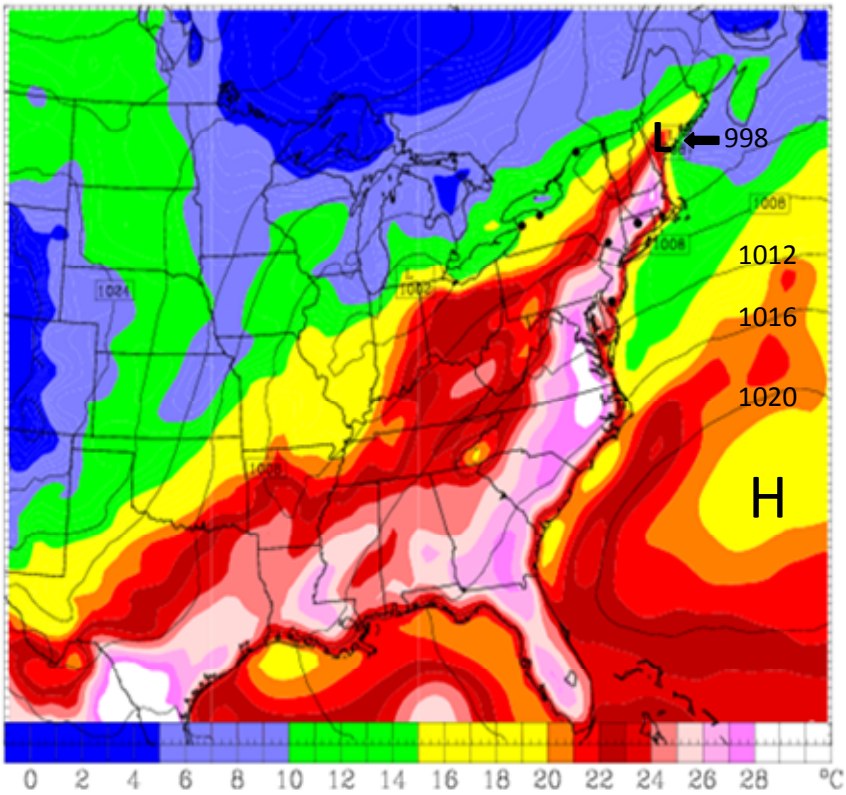

Figure 3.34. Results of the control run for the 7-8 2010 event. The forecast hour is 2100 UTC on 7 April 2010. MSLP (solid line, contoured every 4 hPa), and 2-meter temperature (shaded). The center of the surface high and low pressure systems are labeled with H and L respectively. The 998 denotes the strength of the surface low pressure over southern ME.

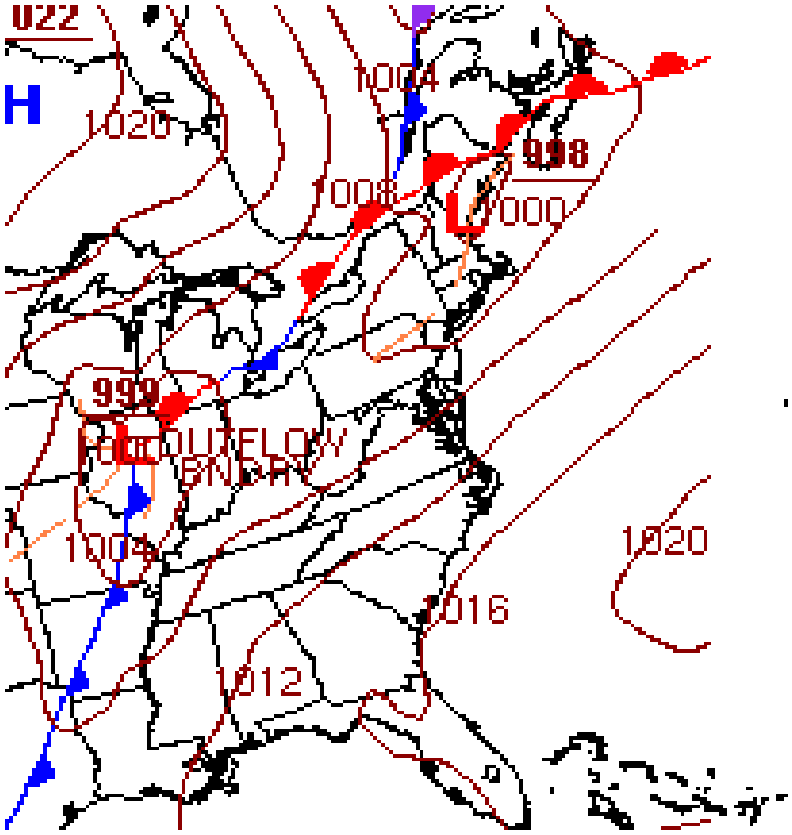

Figure 3.35. Surface analysis for 2100 UTC on 7 April 2010 from the Hydrometeorological Prediction Center (HPC) with MSLP in hPa (solid, contoured every 4 hPa), warm front is labeled as a red line with red semi-circles, cold front is labeled with a blue line with blue triangles, stationary front is labeled as an alternating red and blue line with alternating red semi-circles and blue triangles, and trough is labeled as a dashed orange line.

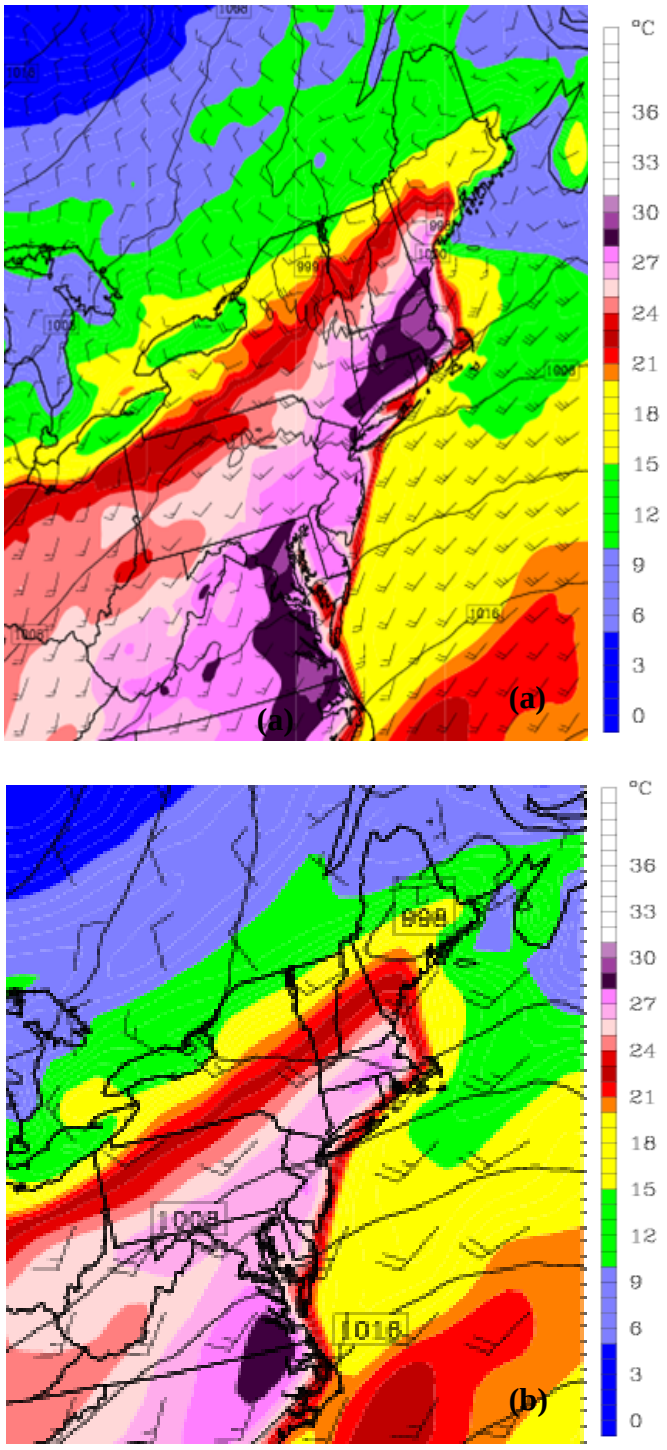

Figure 3.36. (a) Results of the control run for 7-8 April 2010 event. The forecast hour is 2100 UTC on 7 April 2010. MSLP in hPa (solid line, contoured every 4 hPa), 2-meter temperature (shaded), and 10-meter wind (barbs, half wind barb is 2.5 m s^{-1}, full wind barb is 5 m s^{-1}). (b) same as in a) but for the NO_TER experimental run.

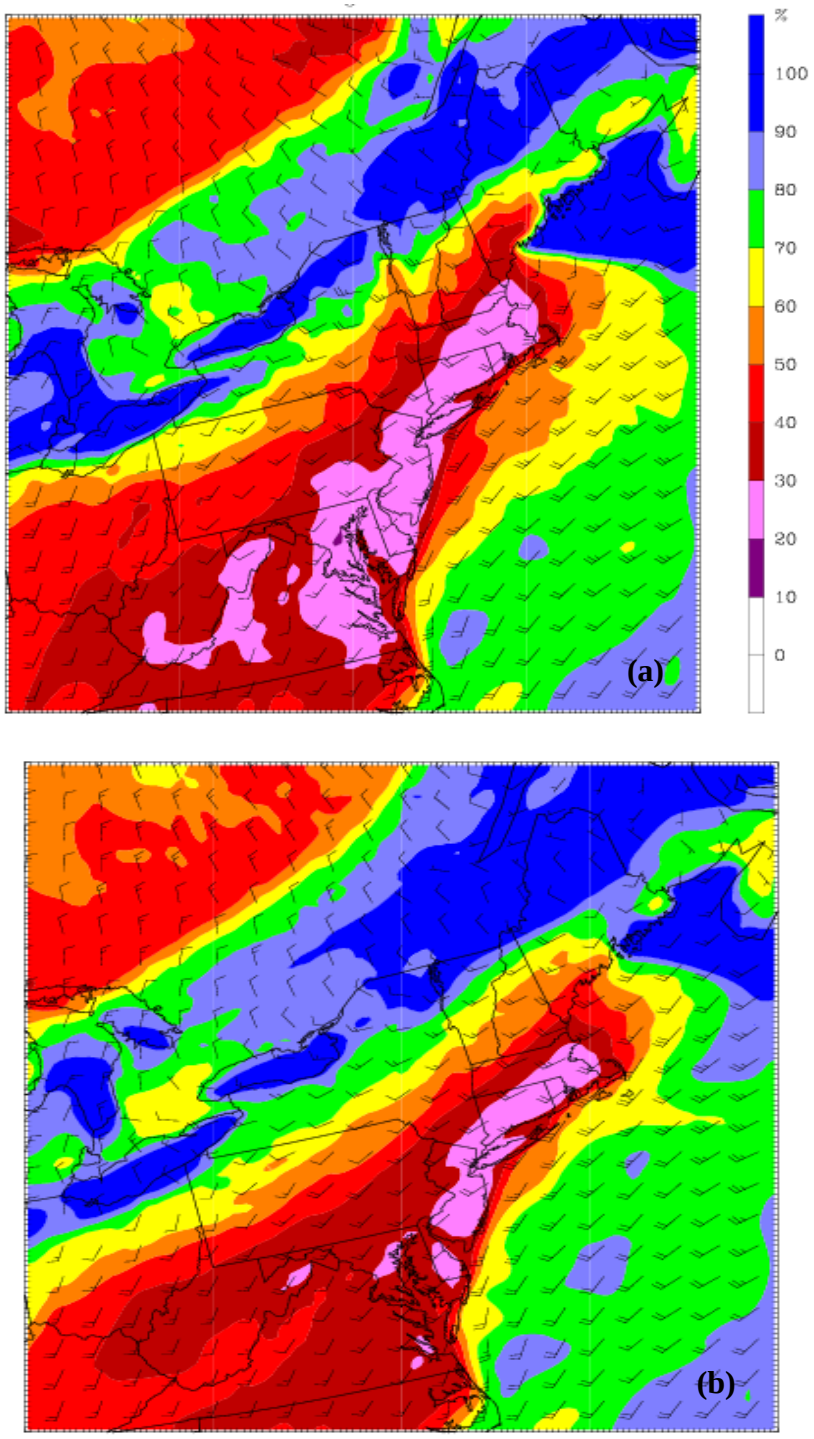

Figure 3.37. (a) Results of the control run for 7-8 April 2010 event. The forecast hour is 2100 UTC on 7 April 2010. 2-meter RH (shaded) and 10-meter wind (barbs, half wind barb is 2.5 m s^{-1}, full wind barb is 5 m s^{-1}). (b) same as in a) but for the NO_TER experimental run.

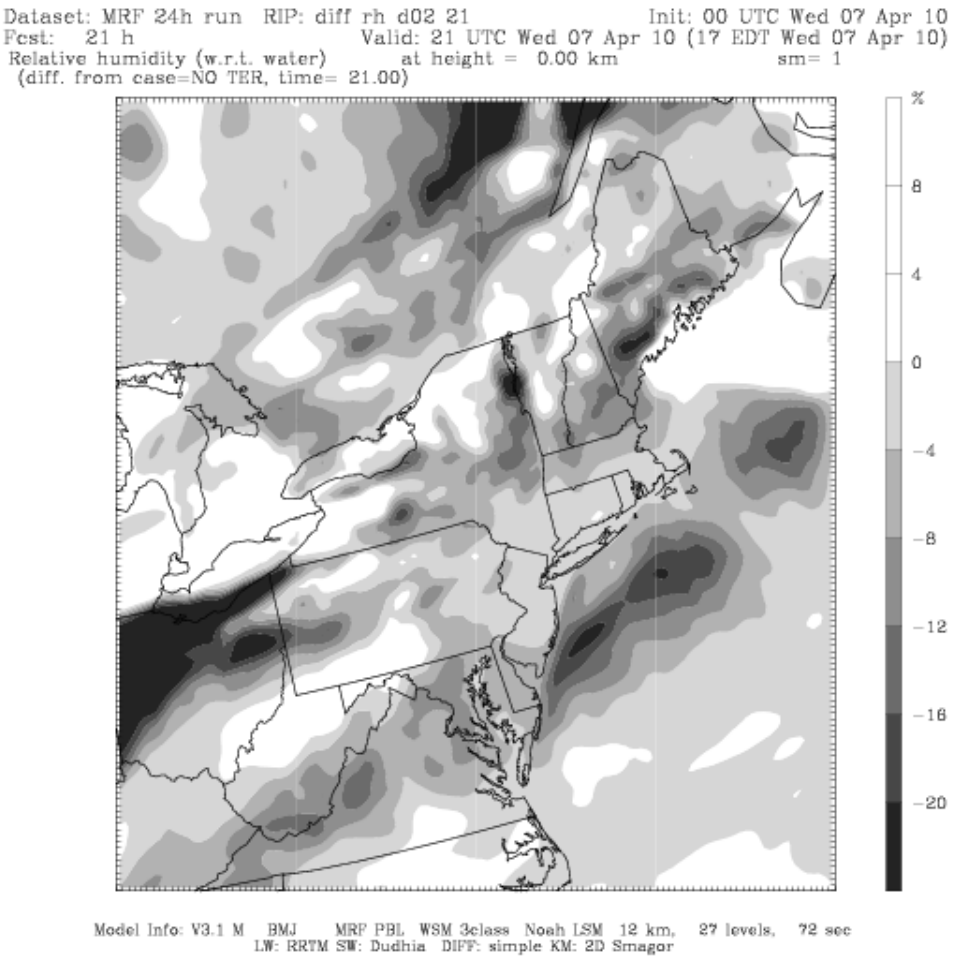

Figure 3.38. Percent difference in RH values between the control run and the NO_TER experimental run for April 7 2010 at 2100 UTC.

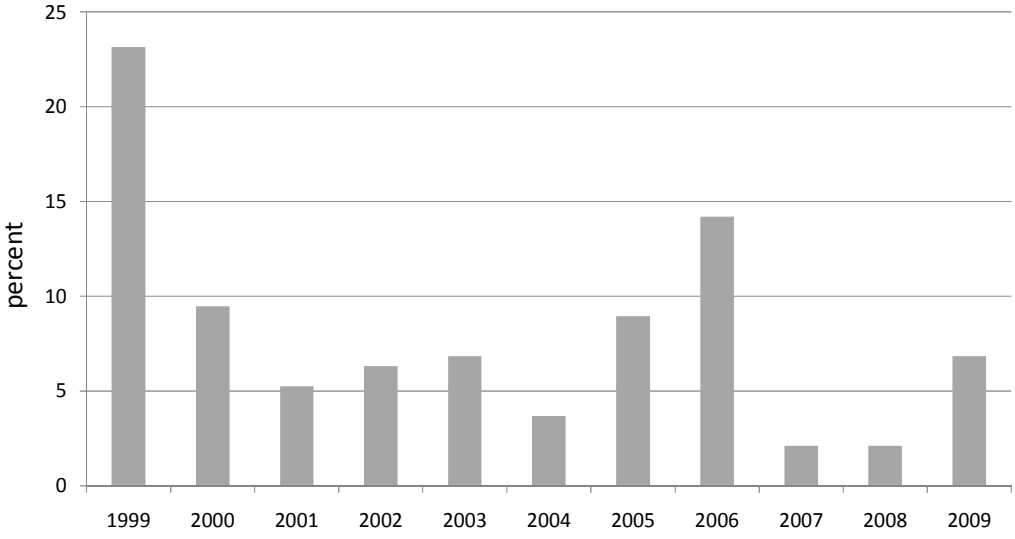

Figure 3.39. Annual wildfire threat climatology for the entire NEUS.

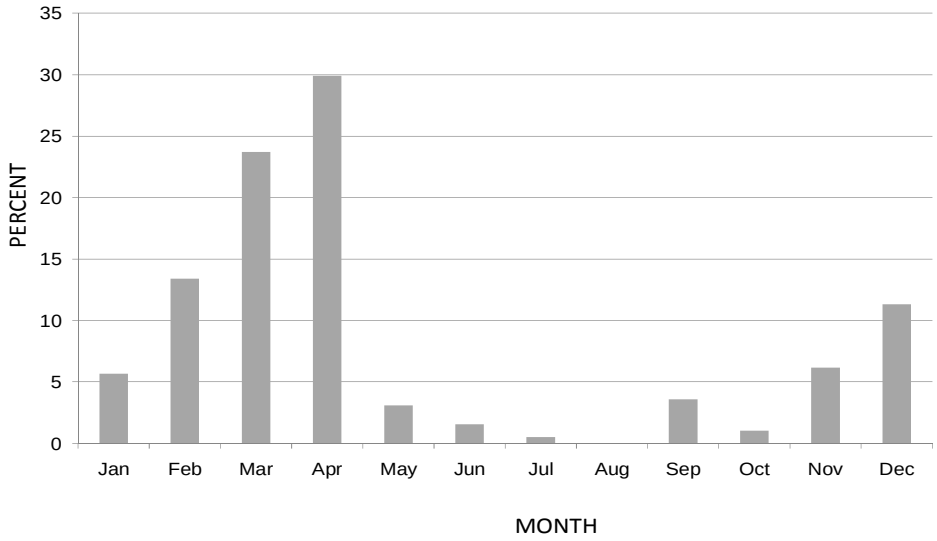

Figure 3.40. Monthly climatology for the entire NEUS for wildfire threat days.

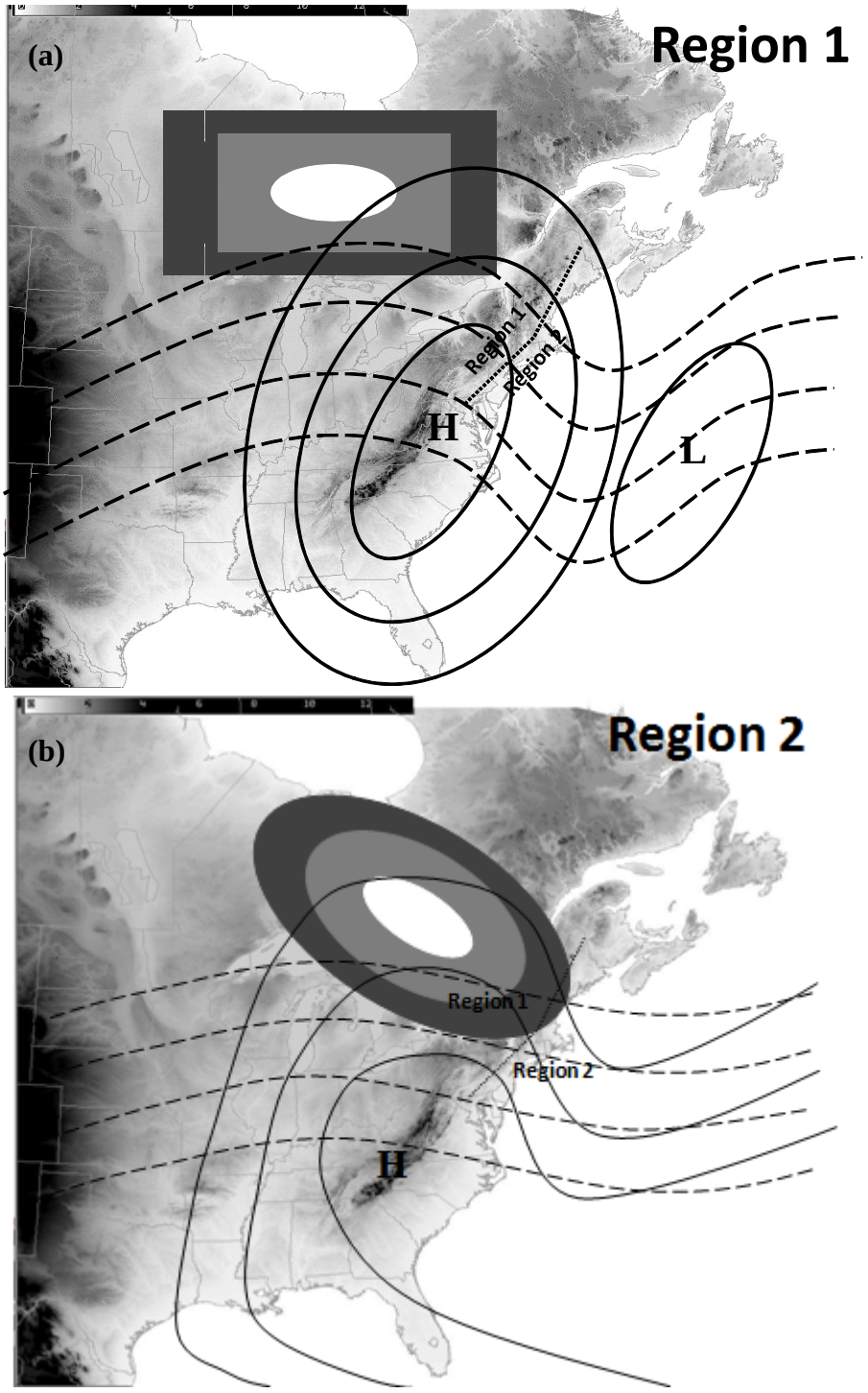

Figure 3.41. Conceptual models on a topographical map for (a) region1 and (b) region 2 showing surface highs and lows labeled H and L respectively, MSLP (solid lines), 500 hPa heights (long dashed lines) and 300 hPa jet core (shaded, higher values are lighter shades). Region 1 and region 2 are divided by the short dashed line.

References

Atger, F., 2003: Spatial and interannual variability of the reliability of ensemble-based probabilistic forecasts: Consequences for calibration. *Mon. Wea. Rev.,* **131,** 1509–1523.

Avissar, R. and R. Pielke, 1989: A parameterization of heterogeneous land surfaces for atmospheric numerical models and its impact on regional meteorology. *Mon. Wea. Rev.*, **117,** 2113-2136.

Barriopedro, D. and Garcia-Herrera R.: A climatology of northern hemisphere blocking. *Journal of Climate*, **19,** 1042-1063.

Bennett, M., 1995. A Lidar study of the limits to plume rise in a well-mixed boundary layer.

Atmospheric Environment, **29**, 2275-2288.

Brockway, D. G., R. G. Gatewood, and R. B. Paris. 2002. Restoring fire as an ecological process in shortgrass prairie ecosystems: initial effects of prescribed burning during the dormant and growing seasons. *Journal of Environmental Management* **65**, 135-152.

Brotak EA, Reifsnyder WE (1977) An investigation of the synoptic situations associated with major wildland fires. *Journal of Applied Meteorology* **16**(9), 867-870.

Buckley, C., 2008: Forest Fire Scorches 3,000 Acres in Ulster Park. The New York Times. [Available online at http://www.nytimes.com/2008/04/21/nyregion/21minnewaska.html?ref=nyregion].

Buizza, R., 1997: Potential forecast skill of ensemble prediction and spread and skill distributions of the ECMWF ensemble prediction system. *Mon. Wea. Rev.,* **125,** 99–119.

Canadian Wildland Fire Information System, 2007: Canadian wildland fire information system. [Available online at http://cwfis.cfs.nrcan.gc.ca/en/index_e.php].

Charney, J. J., X. Bian, B. E. Potter, and W. E. Heilman, 2003: The role of a stratospheric intrusion in the evolution of the Double Trouble State Park wildfire. *Proceedings, 5th Symposium on Fire and Forest Meteorology*, Orlando, FL, 16-20 November, 2003.

Charney, J. J. and L. A. Fusina, 2006: Employing numerical weather models to enhance fire weather and fire behavior predictions. *USDA Forest Service Proceedings RMRS-P-41*.

Charney, J. J. and D. Keyser, 2009: Mesoscale model simulation of the meteorological conditions during the 2 June 2002 Double Trouble State Park wildfire. *International Journal of Wildland Fire.* **(19)** 4, 427-448.

Chen, F., 2005: Variability in global land surface energy budgets during 1987-1988 simulated by an off-line land surface model. *Climate Dynamics.* **24**(7-8), 667-684.

Chen, F. and R. Avissar, 1994a: The impact of land-surface wetness on mesoscale heat fluxes. *J. Appl. Meteor.* **33**, 1324-1340.

————and————, 1994b: Impact of land-surface moisture variability on local shallow convective cumulus and precipitation in large-scale models. *J. Apple. Meteor.* **33,** 1382-1401.

———— and J. Dudhia, 2001: Coupling an advanced land surface hydrology model with the Penn State–NCAR MM5 modeling system. Part I: Model implementation and sensitivity. *Mon. Wea. Rev.,* **129,** 569–585.

Colle, B., 2001: SUNY Stony Brook MM5 numerical forecast information. [Available online at http://atmos.msrc.sunysb.edu/html/info.html].

Crimmins MA (2006) Synoptic climatology of extreme fire-weather conditions across the southwest United States. International Journal of Climatology 26(8), 1001–1016.

Desborough, C.E., 1999: Surface energy balance complexity in GCM land surface models. *Climate Dynamics.* **15**(5), 398-403.

Dudhia, J., 1993: A nonhydrostatic version of the Penn State/NCAR Mesoscale Model: Validation tests and simulations of an Atlantic cyclone and cold front. *Mon. Wea. Rev.,* **121,** 1493–1513.

Draxler, R.R. and G.D. Rolph, 2003: HYSPLIT model access via NOAA ARL READY website (http://ww.arl.noaa.gov/ready/hysplit4.html). NOAA Air Resources Laboratory, Silver Spring, MD.

Eckel, F.A., and C. F. Mass, 2003: Towards an effective short-range ensemble forecast system. *Proc. Workshop on Ensemble Forecasting,* Val-Morin, QC, Canada. [Available online at http:// www.cdc.noaa.gov/people/tom.hamill/ef_workshop_2003.html.].

————, and ————, 2005: Aspects of effective short range ensemble forecasting. *Wea. Forecasting*, **20**, 328–350.

Enloe, Jesse: Plot time series national oceanic and atmospheric administration national climatic data center, retrieved March 3, 2011 [Available online at http://www.ncdc.noaa.gov/temp-and-precip/time-series/]

Enloe, Jesse: State of the climate national oceanic and atmospheric administration national climatic data center, retrieved January 5, 2010 [Available online at http://www.ncdc..noaa.gov/sotc/]

Fosberg, M.A. 1978: Weather in wildland fire management: the fire weather index.

Proceedings of the Conference on Sierra Nevada Meteorology, South Lake Tahoe,

NV. pp. 1-4.

Glickman, T., 2000: *Glossary of Meteorology*. 2nd ed. Amer. Meteor. Soc., 855 pp.

Grell, G.A., 1993: Prognostic evaluation of assumptions used by cumulus parameterizations. *Mon. Wea. Rev.*, **121**, 764-787.

Grimit, E. P., and C. F. Mass, 2002: Initial results of a mesoscale short-range ensemble forecasting system over the Pacific Northwest. *Wea. Forecasting,* **17,** 192–205.

Haines, Donald A., 1988: A lower atmosphere severity index for wildlife fires. *National Weather Digest.* **13**(2): 23-27.

Hamill, and S. J. Colucci, 1997: Verification of Eta–RSM shortrange ensemble forecasts. *Mon. Wea. Rev.*, **125,** 1312–1327.

Hamilton and Ostapow, 2009: Long Island, NY - Central Pine Barrens. National Database of State and Local Wildfire Hazard Mitigation Programs, USDA Forest Service. [Available online at http://www.wildfireprograms.com/search.html?search=advanced&string=SUNRISE%20FIRE&state=&displayId=283].

Hamm, A., Elmore, K., 2003: A Validation of the National Centers for Environmental Prediction's Short Range Ensemble Forecast. *20th Conference on Weather Analysis and Forecasting/16th Conference on Numerical Weather Prediction*. [Available online at http://www.caps.ou.edu/reu/reu03/papers/Andy.pdf.

Hardy, C., R.D. Ottmar, J. Peterson, and J. Core: 2002. Smoke management guide for prescribed and wildland fire -- 2000 edition. Boise, ID: National Wildfire Coordinating Group.

Heffter J.L., 1980: Transport Layer Depth Calculations. *Proceedings 2nd Joint Conference on Applications of Air Pollution Modeling.* AMS, pp. 787-791.

Hoadley, J. L., K. Westrick, S. A. Ferguson, S. L. Goodrick, L. Bradshaw, and P. Werth, 2004: The effect of model resolution in predicting meteorological parameters used in fire danger rating. *J. Appl. Meteor.*, **43,** 1333–1347.

Holzworth C.G., 1967: Mixing depths, wind speeds and air pollution potential for selected locations in the United States. *J. Appl. Meteorol*. **6**, 1039-1044.

Hydrometeorological Prediction Center, 2009: HPC's surface analysis archive. [Available online at http://www.hpc.ncep.noaa.gov/html/sfc_archive.shtml].

Jones, M. S., B. A. Colle, and J. S. Tongue, 2007: Evaluation of a mesoscale short-range ensemble forecast system over the Northeast United States. *Weather and Forecasting*, **22**, 36 – 55.

Kaplan, M.L., C. Huang, Y.L. Lin, and J. J. Charney, 2008: The development of extremely dry surface air due to vertical exchanges under the exit region of a jet streak. *Meteorology and Atmospheric Physics*, **102**:63–85.

Keetch, J. J. and G.M. Byram, 1968: A drought index for forest fire control. *U.S.D.A. Forest Service Research Paper SE-38.*

Kassomenos, Pavlos, 2010: Synoptic circulation control on wild fire occurrence, Physics and Chemistry of the Earth, Parts A/B/C, Volume 35, Issues 9-12, Classifications of Atmospheric Circulation Patterns - Theory and Applications, Pages 544-552.

Li, M., Qu, J., Hao, Xi, 2010: Monitoring temporal and spatial variations of vegetation phenology from space. [Available online at http://spie.org/documents/Newsroom/Imported/003242/003242_10.pdf]

Mesinger, F., G. DiMego, E. Kalnay, P. Shafran, W. Ebisuzaki, D. Jovic, J. Woollen, K. Mitchell, E. Rogers, M. Ek, Y. Fan, R. Grumbine, W. Higgins, H. Li, Y. Lin, G. Manikin, D. Parrish, and W. Shi, et al., 2006: A long-term, consistent, high-resolution climate dataset for the North American domain, as a major improvement upon the earlier global reanalysis datasets in both resolution and accuracy. *Bull. Amer. Meteor. Soc*., **87** (3), 343-360.

Menut, L., C. Flamant, J. Pelon, and P. Flamant, 1999: Urban boundary-layer height determination from lidar measurements over the Paris area. *Appl. Opt*., **38** (6), 945-954.

Mills, G.A., 2005: On the sub-synoptic scale meteorology of two extreme fire weather days during the Eastern Australian fires of January 2003. *Aust. Meteor. Mag.* **54**, 265-290.

Minnesota Department of Natural Resources, Section of Wildlife, 2008: The benefits of prescribed burning on private land. [Available online at http://files.dnr.state.mn.us/assistance/backyard/privatelandsprogram/benefits_prescribed_burning.pdf].

Mölders, N., 2008: Suitability of the Weather Research and Forecasting (WRF) model to predict the June 2005 fire weather for Interior Alaska. *Wea. Foreast*. **23**(5), 953-973.

Morrin, Tim, 2009. Interview by J. Pollina [live interview]. Observation Program Leader with the National Weather Service, New York, NY.

National Drought Mitigation Center, 2011: U.S. Drought Monitor, published online July 6, 2011 from http://droughtmonitor.unl.edu/archive.htlm, retrieved July 7, 2011.

National Interagency Fire Center, 2008: Fire information – wildland fire statistics. [Available online at http://www.nifc.gov/fire_info/ytd_state_2008.htm].

National Wildfire Coordination Group, 1994: Intermediate wildland fire behavior student workbook. Available through the National Interagency Fire Center.

National Weather Service, WFO-New York, 174 Brookhaven Ave. Bldg. NWS-1, Upton, NY 11973. 2008: Ready Reference Binder #7

National Weather Service, WFO-New York: Climatological Data, published online April 7, 2008, retrieved on December 12 2010 [Available online at http://www.erh.noaa.gov/okx/climateindex.php?wfo=okx].

National Weather Service, WFO-New York: Climatological Data, published online August 14, 2010, retrieved on May 6 2011[Available online at http://www.erh.noaa.gov/okx/climate_cms.html#Historical

Newark M.J. (1975) The relationship between forest fire occurrence and 500 hPa longwave ridging. *Atmosphere* , **13**(1), 26-33.

Nimchuk N (1983) Wildfire behavior associated with upper ridge breakdown. Alberta Energy and Natural Resources Forest Service Report No. T/50. (Edmonton, Alberta)

NOAA National Climatic Data Center, State of the Climate: National Overview for March 2000, published online April 2000, http://www.ncdc.noaa.gov/sotc/?report=national&year=1999&month=15.

NOAA National Climatic Data Center, State of the Climate: National Overview for April 2000, published online May 2000, retrieved on October 31, 2010 from http://www.ncdc.noaa.gov/sotc/?report=national&year=1999&month=16.

Novak, D.R. and Colle, B.A., 2006: Observations of multiple sea breeze boundaries during an unseasonably warm day in metropolitan new york city. *Bulletin of the American Meteorological Society*, **87**(2), 169-174

Parr, Dr. K., Dr. L. Instone, Dr. P. Wurm, H. Rysavy, Dr. D. Williams, L. Coleman, Dr. L. Prior, R. Mercer, R. Jalil, Dr. S. Setterfield, Dr. J Luly, and Dr. M Page, 2005: Fire ecology and management in northern australia. Tropical Savannas CRS and Bushfire CRC. [Available online at http://learnline.cdu.edu.au/units/sbi263/fundamentals/fundamentals.html].

Plymouth State Weather Center, 2009: Welcome to the Plymouth state weather center! [Available online at http://vortex.plymouth.edu/].

Radtke, K.W.-H, Arndt, A.M., and Wakimoto, R.H. 1982: Fire history of the santa monica mountains. USDA Forest Service, Pacific Southwest Forest and Range Experiment Station, PSW-58. Technical Report. 438-443. (Berkeley, CA)

Raphael, M.N., 2003: The Santa Ana winds of California. *Earth Interactions*, **7**, 1-13.

Richardson, D. S., 2001: Ensembles using multiple models and analyses. *Quart. J. Roy. Meteor. Soc.*, **127,** 1847–1864.

Roebber, P. J., D. M. Schultz, B. A., and D. J. Stensrud, 2004: Toward improved prediction: High-resolution and ensemble modeling systems in operations. *Wea. Forecasting,* **19,** 936–949.

Rorig, M.L, and Ferguson, S.A., 2002: The 2000 fire season: lightning-caused fires. *Journal of Applied Meteorology.* **41**(7), 786-791.

Saltenberger, John, 2003: Notes on the haines index. Fire Weather Office, Northwest Interagency Coordination Center. [Available online at http://www.wrh.noaa.gov/sew/fire/olm/haines.htm].

Sasano, Y. 1985: Observational study on the atmospheric mixed layer and transition layer structures using Mie lidar. *Journal of the Meteorological Society of Japan*, **63**, 419-435.

Schaefer VJ (1957) The relationship of jet streams to forest wildfires. *Journal of Forestry* **55**(6), 419-425.

Schroeder MJ, Glovinsky M, Hendricks VF [and others] (1964) Synoptic weather types associated with critical fire weather. Defense Documentation Center For Scientific and Technical Information, Cameron Station Alexandria, VA. USDA Forest Service, Pacific Southwest Forest and Range Experiment Station, (Berkeley, California).

Shein, Karsten, 2009: Climate of 2008 wildfire season summary. [Available online at: http://www.ncdc.noaa.gov/oa/climate/research/2008/fire08.html].

Skamarock, W.C., J. B. Klemp, J. Dudhia, D. O. Gill, D. M. Barker, W. Wang, J. G. Powers, 2005: A Description of the Advanced Research WRF Version 2. *NCAR Tech Note, NCAR/TN-468+STR*, 88 pp. [Available from UCAR Communications, P. O. Box 3000, Boulder, CO 80307].

Skinner WR, Flannigan MD, Stocks BJ, Martell DL, Wotton BM, Todd JB, Mason JA, Logan KA, and Bosch EM (2002) A 500 mb synoptic wildland fire climatology from large Canadian forest fires, 1959-1996. *Theoretical and Applied Climatology* **71**(3-4), 157-169.

Skinner WR, Stocks BJ, Martelli DL, Bonsal B, and Shabbar A (1999) The association between circulation anomalies in the mid-troposphere and area burned by wildland fire in Canada. *Theoretical and Applied Climatology* **63**(1-2), 89-105.

Smirnova, T. G., J. M. Brown, and S. G. Benjamin, 1997: Performance of different soil model configurations in simulating ground surface temperature and surface fluxes. *Mon. Wea. Rev*., 125, 1870–1884.

Stensrud, D. J., H. E. Brooks, J. Du, M. S. Tracton, and E. Rogers, 1999: Using ensembles for short-range forecasting. *Mon. Wea. Rev.*, **127,** 433–446.

————, D. J., and N. Yussouf, 2003: Short-range ensemble predictions of 2-m temperature and dewpoint temperature over New England. *Mon. Wea. Rev.*, **131**, 2510-2524.

Storm Prediction Center, 2009: Surface and upper air maps. [Available online at http://www.spc.noaa.gov/obswx/maps/].

Strawbridge, K. B. and Snyder, B. J., 2004: Planetary boundary layer height determination during Pacific 2001 using the advantage of a scanning lidar instrument, *Atmos. Environ*., **38**, 5861–5871, 2004.

Takle, E.S., D.J. Bramer, W.E. Hellman, and M. R. Thompson, 1994: A synoptic climatology for forest fires in the NE US and future implications from GCM simulations. *Int. J. Wildland Fire.* **4**(4), 217-224.

Trenberth, K.E., 1978: On the interpretation of the diagnostic quasi-geostrophic omega equation. *Mon. Wea. Rev.*, **106,** 131-137.

United States Forest Service, 2009: Urbanization of forestland in the northeastern U.S. [Available online at http://www.fs.fed.us/ne/fia/studies/LDS/urban_maps/northeastmap.jpg].

University of Washington, 2009: Electronic maproom archive. [Available online at http://www.atmos.washington.edu/data/vmaproom/varchive.cgi].

Vogelezang D.H.P. and A.A.M. Holtslag, 1996: Evaluation and model impacts of alternative boundary-layer height formulations. *Boundary-Layer Meteorol*. **81**, 245-269.

Wagner, C.E. Van, 1979: A laboratory study of weather effects on the drying rate of jack pine litter. *Canadian Journal of Forest Research*. **9** (2), 267-275.

Werth, John, 2003: National fire danger rating system. National Oceanic and Atmospheric Administration/National Weather Service. [Available online at http://www.wrh.noaa.gov/sew/fire/olm/nfdrs.htm#nfdrs6].

Wildland Fire Assessment System, 2009: [Available online at http://wfas.net/].

Yarnal, B. 1993: Synoptic climatology in environmental analysis: a primer. Belhaven Press, London